WASHINGTON UNIVERSITY IN ST. LOUIS

James Mckelvey School of Engineering

Department of Mechanical Engineering and Material Science

Thesis Examination Committee

Ramesh Agarwal, Chair

David Peters

Swami Karunamoorthy

Numerical Investigation of Wind Turbine Airfoils under Clean and Dusty Air Conditions

by

Siyuan Chen

A dissertation presented to the James Mckelvey School of Engineering
of Washington University in St. Louis
in partial fulfillment of the requirements for the degree of
Master of Science

May 2020

St. Louis, Missouri, USA

Table of Contents

List of Figures

Nomenclature

α / *AoA*	=	angle of attack
c_l	=	lift coefficient
c_d	=	drag coefficient
l	=	lift force
d	=	drag force
ρ_{air}	=	density of air
ρ_{particle}	=	density of dust particles
$\dot{m}_p$	=	mass flow rate of particles
μ	=	viscosity of air
Re	=	Reynolds number
Ma	=	Mach number
d_{p}	=	diameter of dust particles
c	=	the chord length of airfoils
Δt	=	time step
$\vec{F}_{\text{other}}$	=	other interaction forces
$\vec{u}_{\text{p}}$	=	velocity of particles
$\vec{u}$	=	velocity of airflow

Acknowledgments

I would like to express my sincere gratitude to those who helped me during my research in Computation Fluid Dynamics laboratory.

My deepest gratitude goes foremost to Professor Ramesh Agarwal for his inspiration, encouragement and guidance throughout my research. His knowledge, experience and patience have helped me to accomplish my research project and thesis in an excellent manner. Without him I would not have the opportunity to explore the academic world of Computation Fluid Dynamics (CFD).

Secondly, I would like to express my heartfelt gratitude to Da Xiao, Tianshu Wen and Junhui Li for all their efforts to help me. The patient instruction by Da Xiao and Tianshu Wen played a vital role in initiating my research. The careful guidance of Junhui Li helped me to successfully improve the quality of the mesh and apply discrete phase model to the simulation of flows with dusty air.

Finally, I would like to thank all the instructors, thesis examination committee and group members in CFD lab. It is the harmonious communication environment and exchanging of different ideas that allowed me to keep learning and making progress.

Siyuan Chen

Washington University in St. Louis
May 2020

Dedication

I would like to dedicate this thesis to my father (Jingsong Chen), my mother (Aiqi Zhang) and my fiancée (Yun Wang) for their unconditional support.

I will never succeed without their support, influence and encouragement.

Numerical Investigation of Wind Turbine Airfoils under Clean and Dusty Air Conditions

Siyuan Chen

Master of Science in Mechanical Engineering

Washington University in St. Louis, 2020

Research Advisor: Professor Ramesh K. Agarwal

Abstract of Thesis

The focus of research in this thesis is on numerical simulation of airflow around wind turbine airfoils (S809, S814 and S1210) under both clean and dusty air conditions by using Computational Fluid Dynamics (CFD). The physical geometries of the airfoils and the meshing processes are completed in the ANSYS Mesh package ICEM. The simulations and post-processing are done by ANSYS FLUENT. For cases of clean air condition, Spalart–Allmaras (SA), realizable k-ε and Wray-Agarwal (WA) turbulence models are employed in the calculations. The results are compared with the experimental data for validation. For dusty air condition, simulation of the two-phase flow is conducted using the discrete phase model (DPM) for various concentrations of dust particles using the realizable k-ε model and WA turbulence models. The results are compared with the clean air simulations to illustrate the effect of dust contamination on the aerodynamic performance of the airfoils. Finally, some conclusions are drawn on how several factors influence the aerodynamic performance of the airfoils and suggestions are made to improve the wind energy conversion efficiency of airfoils under clean and dusty air conditions.

Chapter 1: Introduction

1.1 Background and Motivation

Due to the environmental concerns related to the increasing carbon dioxide emissions and global warming with use of fossil fuels, there is great deal of interest in exploitation of long-lasting renewable energy sources such as wind energy, biomass, solar energy and ocean energy. In the context of wind energy, considerable amount of research has been conducted on the design of wind turbines and wind farms to extract maximum possible energy from the wind.

Currently there are two most popular types of wind turbines---Horizontal Axis Wind Turbines (HAWT) and Vertical Axis Wind Turbines (VAWT) [1]. To explain the terminology, horizontal axis means the rotating axis of the wind turbine blades is parallel to the ground while vertical axis means that it is perpendicular to the ground. Figure 1 provide the illustration of physical structure of HAWT and VAWT. Both horizontal and vertical axis wind turbines have advantages and disadvantages. For instance, HAWT can generate more electricity from a given amount of wind than VAWT. However, the equipment of HAWT is more complex and heavier, which increases the cost of production and transportation. Furthermore, experimental results show that the aerodynamic performance of HAWT degrades in turbulent wind conditions. Nevertheless, horizontal axis wind turbines dominate the power requirement of the wind energy industry while vertical axis wind turbines are primarily used in relatively small and residential applications. Hence the investigation and optimization of aerodynamic performance of HAWT has been significantly pivotal in wind energy industry. Several wind turbine airfoils and blades have been studied and newer airfoils/blades are being analyzed in the literature. National Renewable Energy Laboratory (NREL) in Colorado and National Advisory Committee for Aeronautics (NACA) have led the effort in this research along with industry and academia. The research at

Rajshahi University has shown the comparison and difference between NACA and NREL families of airfoils. It turns out that NACA airfoils have better average aerodynamic performance whereas NREL airfoils demonstrate higher level of stability and durability at higher wind speeds [2, 3].

In case of HAWT, NREL S-series airfoils are representative of many horizontal axis wind turbine airfoils, for example, aerodynamic characteristics of S809 airfoil have been extensively studied in literature. There are also other S-series airfoils of different thicknesses and cambers with different lift and drag characteristics. This paper focuses on three S-series airfoils, which includes S809 airfoil, S814 airfoil and S1210 airfoil. These three airfoils differ in their aerodynamic performance. These airfoils have been separately tested in wind tunnels at the Delft University of Technology, the Ohio State University and the University of Illinois at Urbana-Champaign. The experimental results have been published [4-7], which are utilized for comparison and validation with the numerical results in this thesis.

Sand-storm weather and dusty air environment is very common in certain parts of the world, e.g. in such as Middle East and the northwest part of China. Wind turbines play a crucial role in generating electricity in these regions. However, in spite of the importance of wind turbines, until now only a limited number of research studies and publications consider the influence of dusty air condition on the aerodynamic performance of wind turbine airfoils, which includes the lift coefficient, drag coefficient and pressure coefficient of airfoils. In 2017, Douvi, Margaris and Davaris published a paper considering the effect of dusty air effect on the aerodynamic performance of S809 airfoil [8]. The goal of this paper was to investigate the detrimental effect of dust particles on the aerodynamic performance of S809 airfoil and use the study to suggest improvements to increase the energy efficiency of wind turbines under dusty air conditions.

Figure 1: Horizontal axis wind turbine (left) and vertical axis wind turbine (right)

1.2 Scope of the Thesis

The main focus of this thesis is on the evaluation of the aerodynamic performance of S809, S814 and S1210 airfoils under both clean air condition and dusty air condition by numerical simulation using the computational fluid dynamics technology. In all simulations, incompressible Reynolds-averaged Navier–Stokes (RANS) equations are solved with one-equation Spalart–Allmaras model, two-equation realizable k-ε model and Wray-Agarwal one-equation model. The discrete phase, which consists of tiny dust particles, is injected into the clean air flow by using discrete phase model (DPM) and its effect is calculated in ANSYS FLUENT.

In Chapter 3, a brief introduction to S809 airfoil is given and then compared results and contours of pressure, velocity and turbulence intensity of the airflow are presented. Computed results from several tuburlence models, namely the SA model, the realizable k-ε model, and Wray-Agarwal 2017m model and WA 2018 model, are compared with the experimental data for validation for both clean and dusty air conditions. The comparison provides information which turbulence model is more suitable for high-Reynolds number 2D airfoil simulations. Chapters 4 and 5 show the simulation and results for S814 airfoil and S1210 airfoil. Some discussion about the effect of the different physical shapes of the airfoils on the aerodynamic performance is given in both chapters 4 and 5. In Chapter 5, by comparing and analyzing the results for both clean and dusty air conditions for flow past three airfoils, conclusions about the effects of various factors on the aerodynamic performance of airfoils are drawn and then the final chapter 6 leads to some suggestions about the future work on wind turbine airfoils.

Chapter 2: Numerical Methodology

2.1 Physical Geometry and Mesh Generation

The geometry models of three airfoils are constructed by extracting the coordinates data from Somers's report [4,5] and Airfoil Tools website [30]. In current research, the chord lengths of all airfoils are taken to be 1m. Geometry construction and mesh generation process are completed in ICEM. As shown in Figure 2, the computational domain consists of a semi-circle part ahead of the airfoil with radius 25m and a rectangle part in the rear of the airfoil with 50m height and 25m width. The airfoil is located at the geometric center of the flow field. Inlet, outlet and airfoil are shown in the figure 2 by arrows. Figure 3 shows the zoomed-in-view of the mesh near the three airfoils. Figure 4 gives the precise measurement of the whole computational domain (x, y) coordinates. Due to the turbulent boundary layer near the surface of the airfoils, mesh in this region is refined, and is much denser than the mesh in the far field, it can be observed in the zoomed-in-view of the mesh in Figure 3. ANSYS package ICEM is used for generating the computational grid. Figure 5 demonstrates that the mesh is of high quality and can be adequate for accurate simulation. The solutions are performed on a series of meshes so that it can be ensured that the solution is mesh independent and the distance of first grid point from the airfoil surface y+ is less than 1.

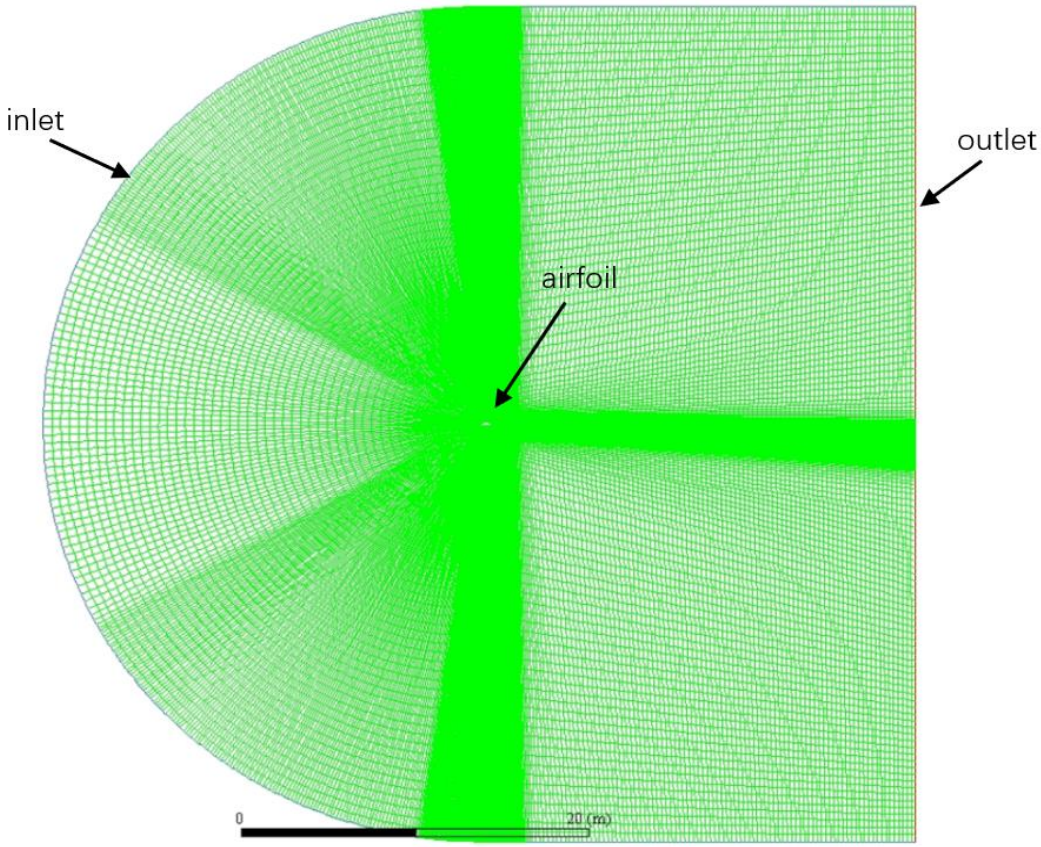

Figure 2: The whole computational domain and mesh around airfoils.

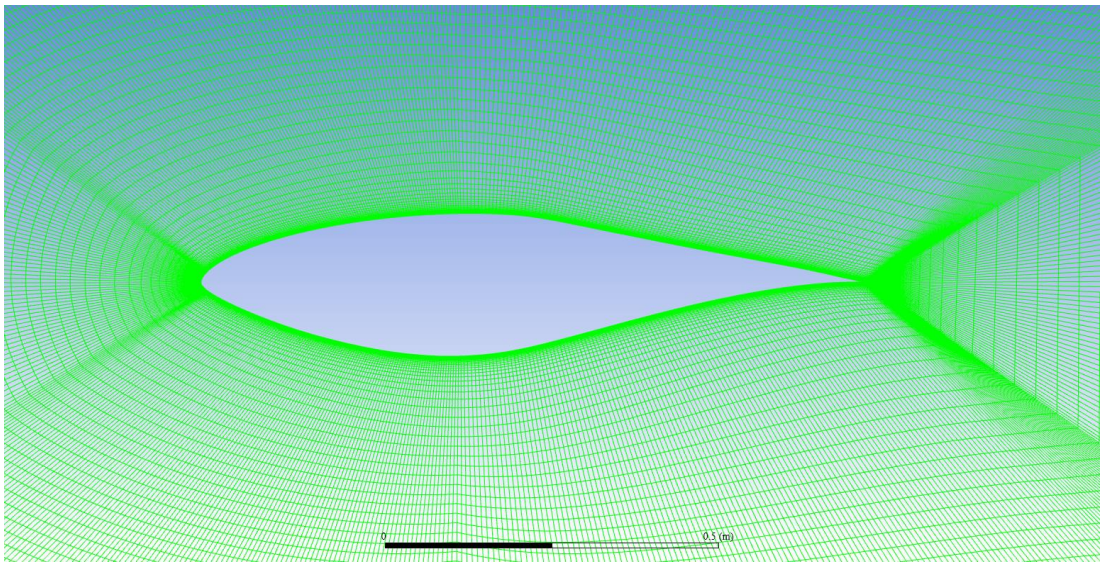

(a) Zoomed-in-view of mesh near S809 airfoil

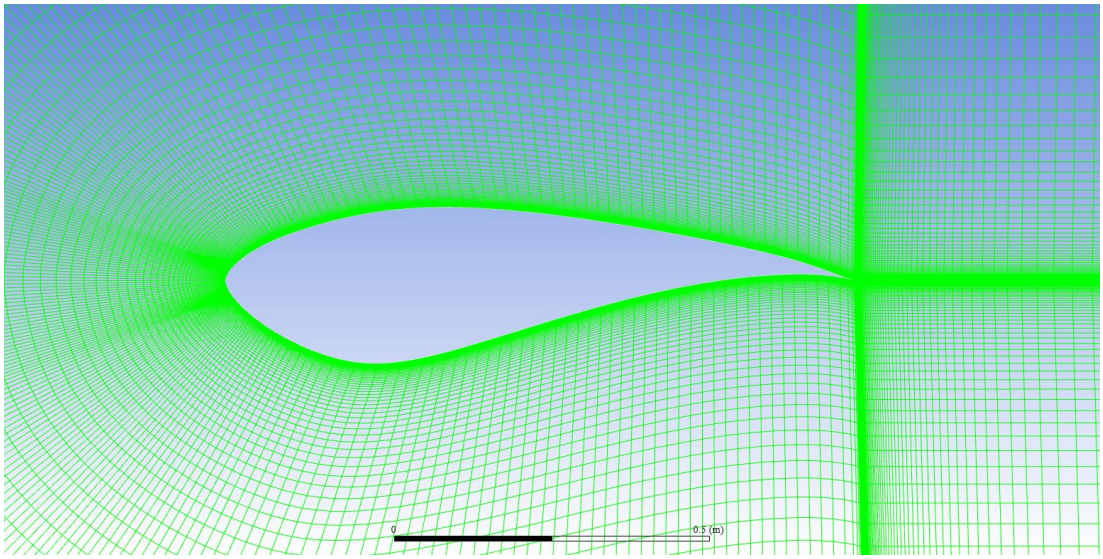

(b) Zoomed-in-view of mesh near S814 airfoil

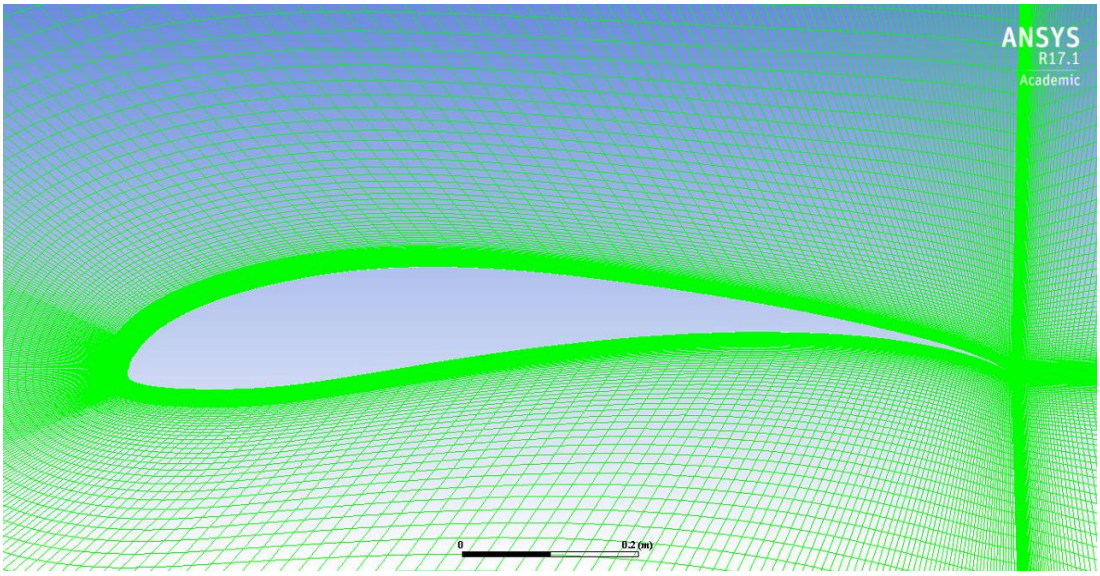

(c) Zoomed-in-view of mesh near S1210 airfoil

Figure 3: Zoomed-in-view of mesh near different airfoils.

Figure 4: Scale of the whole computational domain.

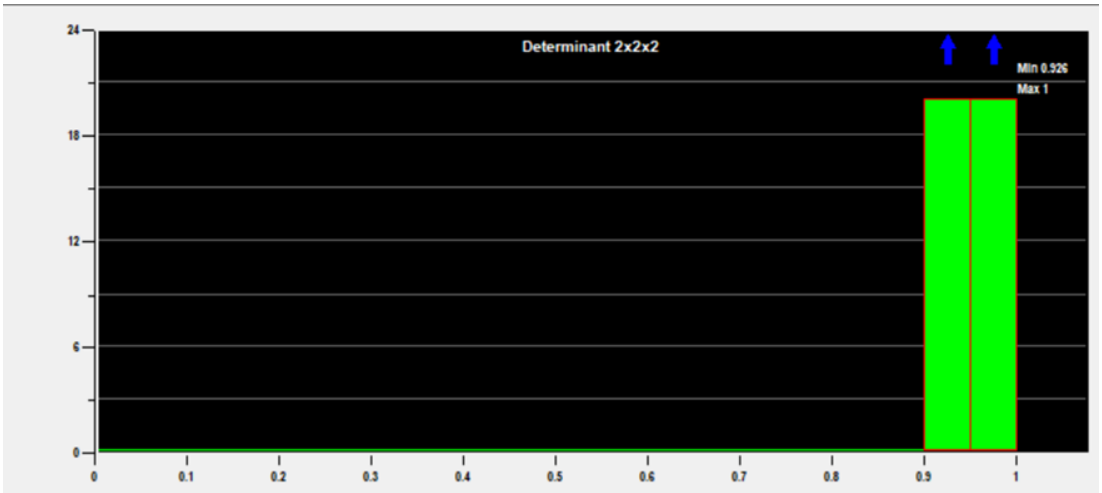

Figure 5: Pre-mesh quality under determinant 2*2*2 criterion.

2.2 Numerical Method and Turbulence Models

Double precision, pressure-based solver in ANSYS FLUENT is chosen for simulation of all cases. For cases of clean air simulations, SA model [9], realizable k-ε turbulence model, WA 2017m model and WA 2018 model [10] are used with the incompressible RANS equations [10-12]. All the model constants of SA model and realizable k-ε model are kept as "default" values in the FLUENT. For cases of dusty air simulations, realizable k-ε model, WA 2017m model and WA 2018 model are chosen for simulations. The discrete phase model (DPM) in FLUENT is employed to inject the dust particles into the flow field, this is one of the most significant steps in this research. No slip wall condition is used on the airfoil solid surface. The inlet is set as velocity-inlet and the outlet is set as pressure-outlet. Coupled scheme for velocity/pressure coupling is applied for solutions of both clean and dusty air conditions.

Spalart-Allmaras (SA) model is a one-equation model developed for aerodynamic flows, such as transonic flow over airfoils including boundary-layer separation [13]. SA model is computationally simpler than two-equation models, therefore this model is wieldy used in industry. The two-equation k-ϵ model is also among the most wieldy used turbulence models to compute many internal and external turbulent flows. This model consists of two transport equations which are solved for two turbulence quantities, k and ϵ. Wray-Agarwal (WA) turbulence model is a one-equation eddy-viscosity model derived from a blended k-ϵ/k-ω formulation. The model performance is better than the commonly used SA model and is comparable to shear stress transport (SST) model for a wide range of canonical flows in aerodynamics [14].

2.3 Discrete Phase Model (DPM)

Currently there are two numerical approaches for calculation of multiphase flows: the Euler-Lagrange approach and the Euler-Euler approach [15]. In the Eulerian-Eulerian approach, the different phases are treated mathematically as interpenetrating continua. Since the volume of a phase cannot be occupied by the other phase, the concept of phase volume fraction is introduced. These volume fractions are assumed to be continuous functions of space and time and their sum is equal to one. In Eulerian-Lagrangian approach, the fluid phase is treated as a continuum by solving the time-averaged Navier-Stokes equations, while the dispersed phase is solved by tracking a large number of particles, bubbles, or droplets through the calculated flow field. The dispersed phase can exchange momentum, mass, and energy with the fluid phase [16]. The change in momentum of a sand particle through each control volume can be calculated by the following equation:

$$F = \sum \left(\frac{18\mu C_D Re}{24\rho_p d_p^2} (u_p - u) + F_{other} \right) \dot{m}_p \Delta t \tag{1}$$

The integration of the force balance on the particle predicts the trajectory of a discrete phase particle. The force balance is written in a Lagrangian reference frame. The forces acting on the particle are equal to the particle inertia and, particularly in the *x* direction, this equality can be expressed as:

$$\frac{du_p}{dt} = F_d(\vec{u} - \vec{u}_p) + \frac{\vec{g}}{\rho_p}(\rho_p - \rho) + \vec{F} \tag{2}$$

$$F_d = \frac{18\mu}{\rho_p d_p^2} \cdot \frac{C_D Re}{24} \tag{3}$$

where $F_d(\vec{u} - \vec{u}_p)$ is the drag force per unit particle mass and $\vec{F}$ is an additional acceleration term per unit particle mass. *Re* is the relative Reynolds number defined as

$$Re \equiv \frac{\rho d_p |\vec{u}_p - \vec{u}|}{\mu} \tag{4}$$

Since the flow is regarded as incompressible and the temperature effects are very small, the energy equation is not considered. For setting the parameters in DPM, surface injection is chosen which means that the dust particles are released into the domain from the inlet boundary of the computational domain and escape from the outlet boundary of the computational domain. The particles are considered inert. The diameter of the particles is 0.001m and the distribution is considered uniform without any agglomeration. The velocity of the particles is the same as the velocity of the air flow. The density of sand particles is ρ_p = 1500kg/m^3. The free stream temperature is 300K, same as the environmental temperature [17].

Chapter 3: S809 Airfoil

3.1 Basic Information of S809 Airfoil

NREL S809 airfoil is a 21-percent-thick, laminar-flow airfoil, which was originated from the 13.5-percent-thick S805 airfoil. Figure 6 shows the geometry of S809 airfoil. It was designed to constrain or limit the maximum lift, reduce the sensitivity to roughness and reduce the increase in drag coefficient due to laminar separation bubbles at the leading edge at high angles of attack. It is also the widely tested and numerically simulated airfoil among S-series of thick-airfoil family.

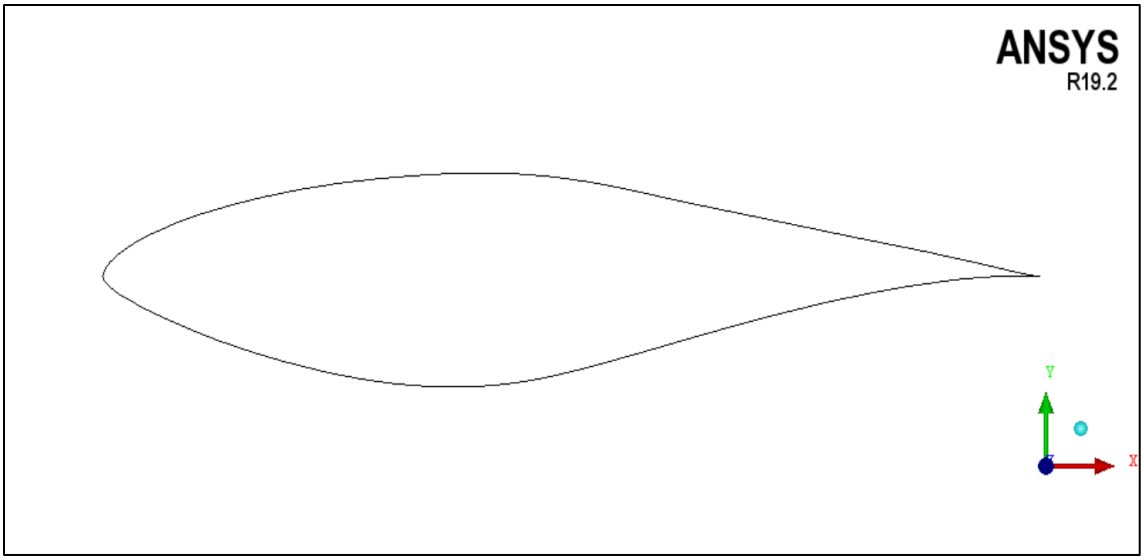

Figure 6: Geometry of S809 airfoil.

3.2 Initial Conditions of the Air Flow

Wind turbine is a typical example of relatively low Reynolds number application. In all cases considered, the Reynolds Number of the flow is $Re = 1\times10^6$, which can be seen as a relatively low Reynolds number, except in one special case which is used for the purpose of comparison case at different Reynolds number [27]. The density of air is ρ_{air}=1.176674 kg/m^3

and the dynamic viscosity of air is μ=1.7894×10^{-5} kg/m·s. All the other parameters are kept as the default value in FLUENT. Mach number is *Ma*=0.066. The initial condition in all computed cases for S814 and S1210 airfoils are the same as that that for the S809 airfoil.

3.3 Simulations and Results under Clean Air Condition

Figures 7 and 8 show the computed aerodynamics characteristics of S809 airfoil using SA model, realizable k-ε model, WA 2017m model and WA 2018 model and their comparison with the experimental data [18]. For S809 airfoil, all four turbulence models show reasonably good agreement with the experimental data for a range of low angles of attack from 0 to 8°. However, as angle of attack increases beyond 8°, it is obvious that there is greater deviation between computed results and the experimental data, and the results of realizable k-ε model and two WA models show better agreement with the experimental data than the SA model which has the largest error. The critical angle of attack for S809 airfoil for Reynolds number = 1 million is about 14°, since at this angle of attack, the lift coefficient reaches its maximum value and then drops significantly due to stall. Besides, it can be observed that when angle of attack is small, the lift coefficient linearly increases with the angle of attack. As angle of attack increases to some larger value, linearly dependence no longer exists and the computed results become more significantly different from the experimental data due to the stall effect [19]. Another interesting fact to note is that the c_l-α curve does not pass through the origin implying that a non-zero lift force exists when angle of attack is zero; this is expected since the airfoil is not symmetrical and has camber [20].

Figure 9 shows the difference in lift coefficient of S809 airfoil at different Reynolds numbers. Since Reynolds number and free stream velocity are linearly dependent with density, length and with viscosity of the fluid being unchanged, different Reynolds numbers imply different free

stream velocities faced by the airfoil. From Figure 9, it can be observed that the lift coefficient increases slightly when the Reynolds number increases from 1×10^6 to 1.5×10^6, which leads to change in the lift to drag ratio. This observation has also been mentioned in other papers [21].

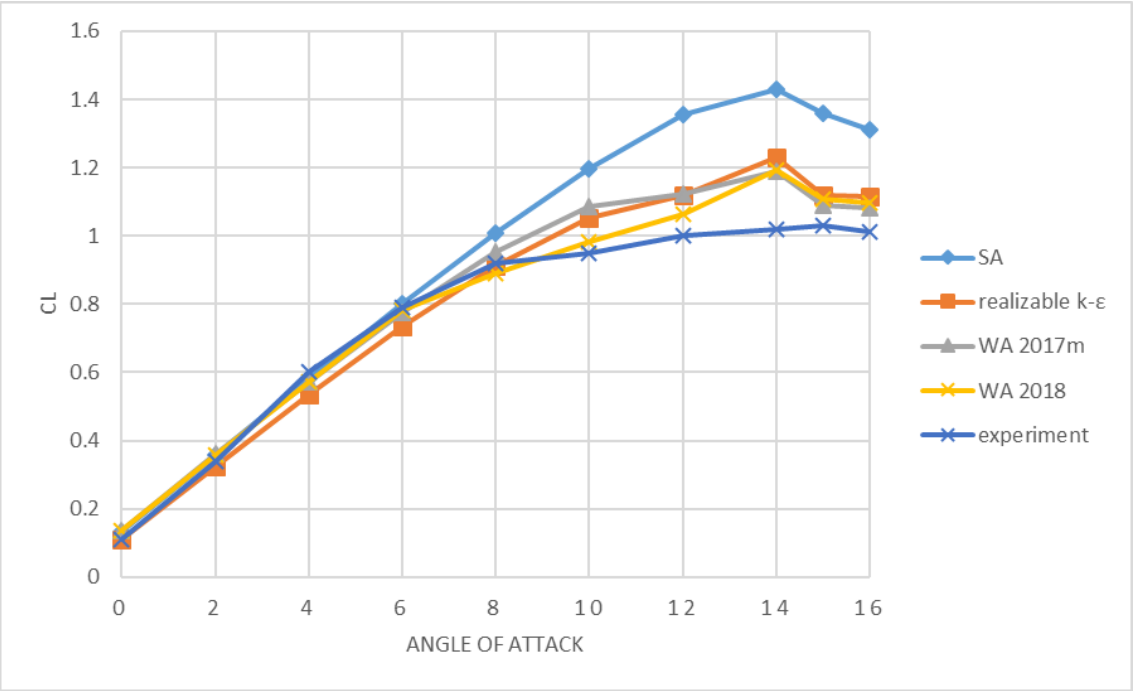

Figure 7: Variation in computed lift coefficients of S809 airfoil under clean air condition using SA model, realizable k-ε model, WA 2017m model and WA2018 model and comparison with experimental data.

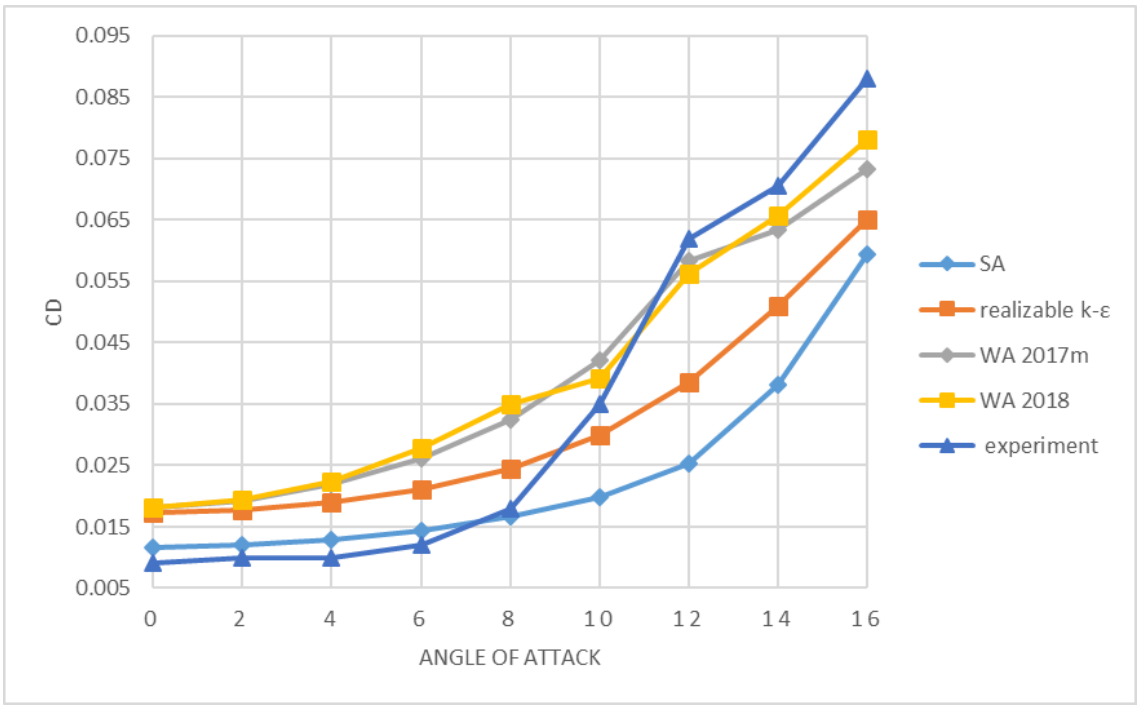

Figure 8: Variation in computed drag coefficients of S809 airfoil under clean air condition using SA model, realizable k-ε model, WA 2017m model and WA2018 model and comparison with experimental data.

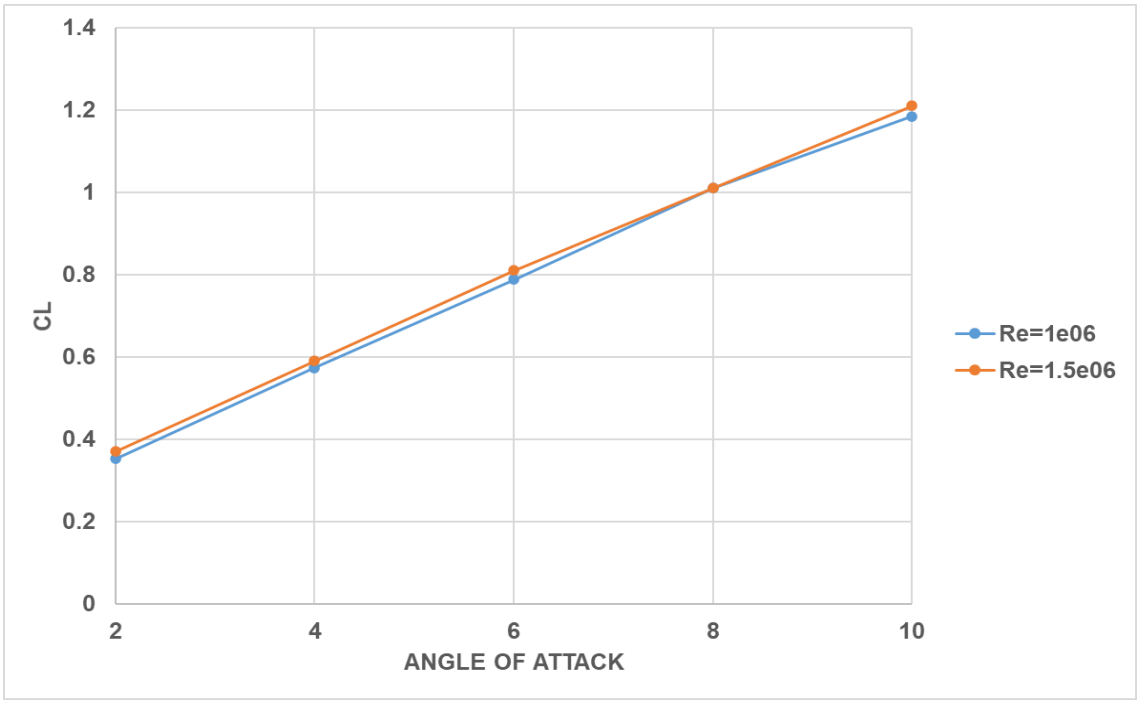

Figure 9: Variation in computed lift coefficient of S809 airfoil with various angle of attack using SA model at different Reynolds Numbers.

3.4 Simulations and Results for Dusty Air Condition

By using discrete phase model(DPM) to inject dust particles into the incoming clean air stream, the effect of solid phase is considered and the results for dusty air condition are computed with realizable k-ε model and WA 2017m model and are compared with experimental data and the results of clean air condition. Figures 10 and 11 show the difference in results using different turbulence models and their agreement with the experimental data. Both turbulence models show good agreement; however WA 2017m model has closer agreement than the realizable k-ε model with experiment data. The comparison in Figures 10 and 11 were performed for concentration of uniform dust particles of 10% by volume. In reality, the concentration of dust particles can vary within a large range depending upon the environment conditions. Hence, computations were performed for different concentrations of dust particles. Figures 12 and 14 illustrate the change in aerodynamic performance under clean air and dusty air with 1%, 10%, 20% and 30% concentration of particles in volume. It can be seen that change in c_l and c_d is very small due to dusty air when angle of attack is small. Figure 13 shows more distinct change in lift coefficient for angles of attack ranging from 4° to 8°. From these figures, it can be concluded that the aerodynamic characteristics of S809 airfoil change depending upon the concentration of dust particles; the lift coefficient decreases and drag coefficient increases with variation in concentration of dust particles as expected. For 1% concentration of dust particles, the change in aerodynamic coefficients is very small and the results are almost the same as the results for clean air. However, for higher concentration of dust particles, some changes in aerodynamic coefficients can be observed and this change becomes larger as the concentration of dust particles increases.

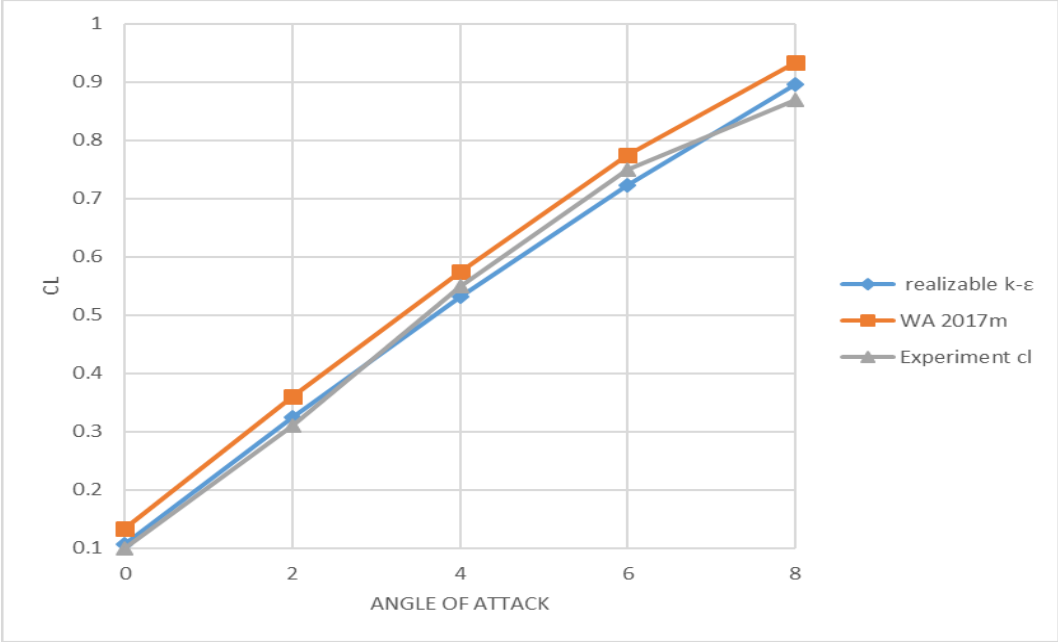

Figure 10: Changes in computed lift coefficient of S809 airfoil under dusty air conditions using realizable k-ε model and WA 2017m model and their comparison with experimental data when concentration of dust particles is 10% in volume.

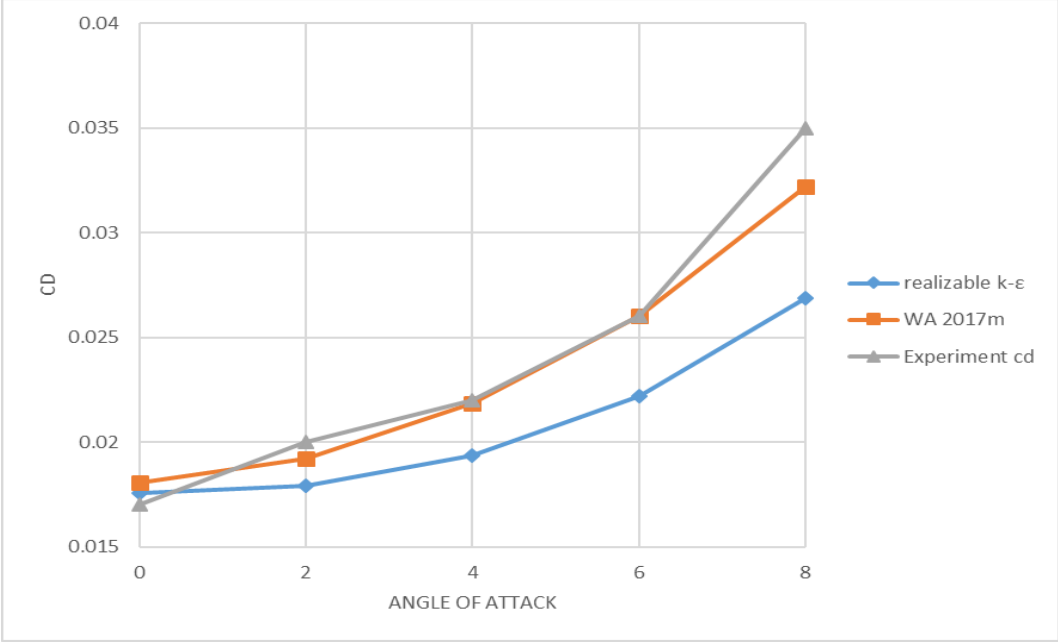

Figure 11: Changes in computed drag coefficient of S809 airfoil under dusty air conditions using realizable k-ε model and WA 2017m model and their comparison with experimental data when concentration of dust particle is 10% in volume.

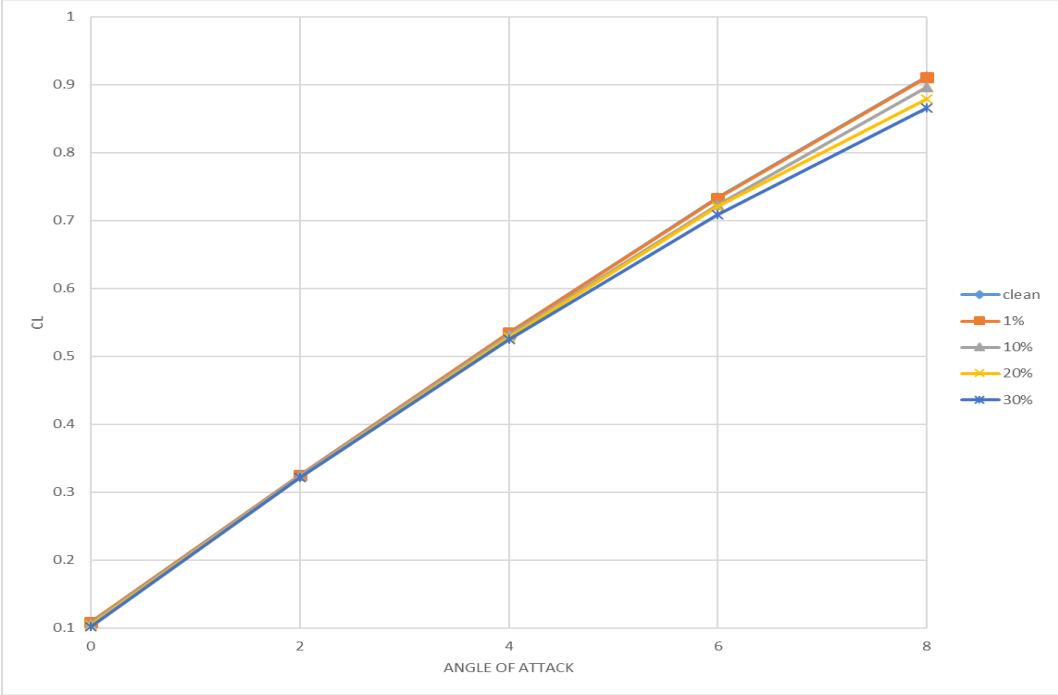

Figure 12: Changes in computed lift coefficient of S809 airfoil under clean air condition for different concentrations of dust particles using realizable k-ε model.

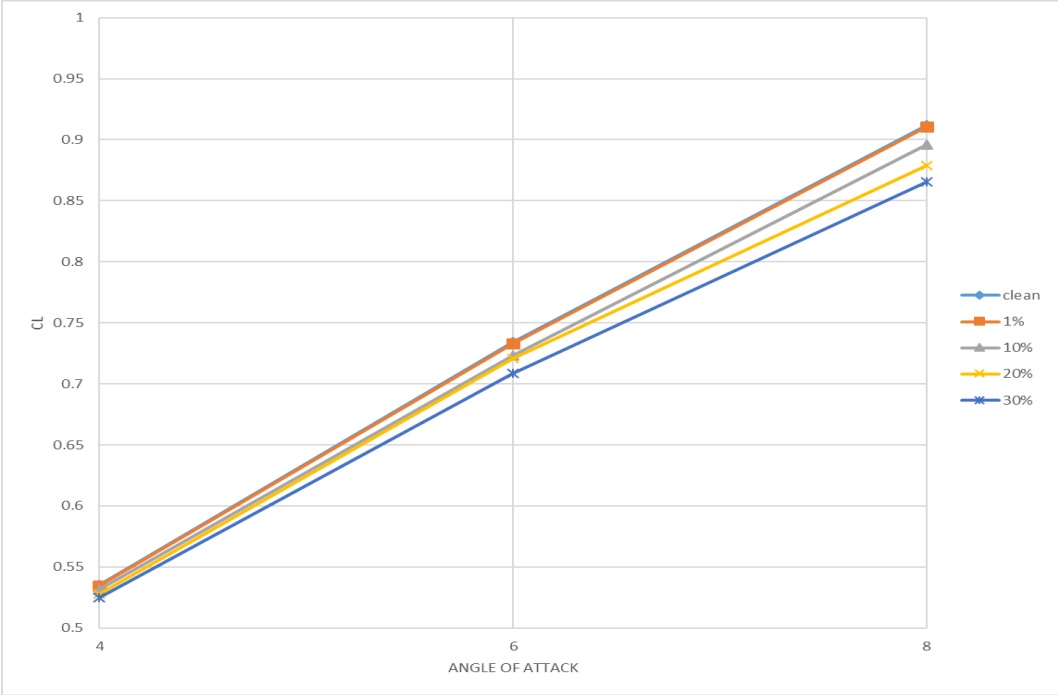

Figure 13: Changes in computed lift coefficient of S809 airfoil for angle of attack range of 4-8° under clean air condition for different concentrations of dust particles using realizable k-ε model.

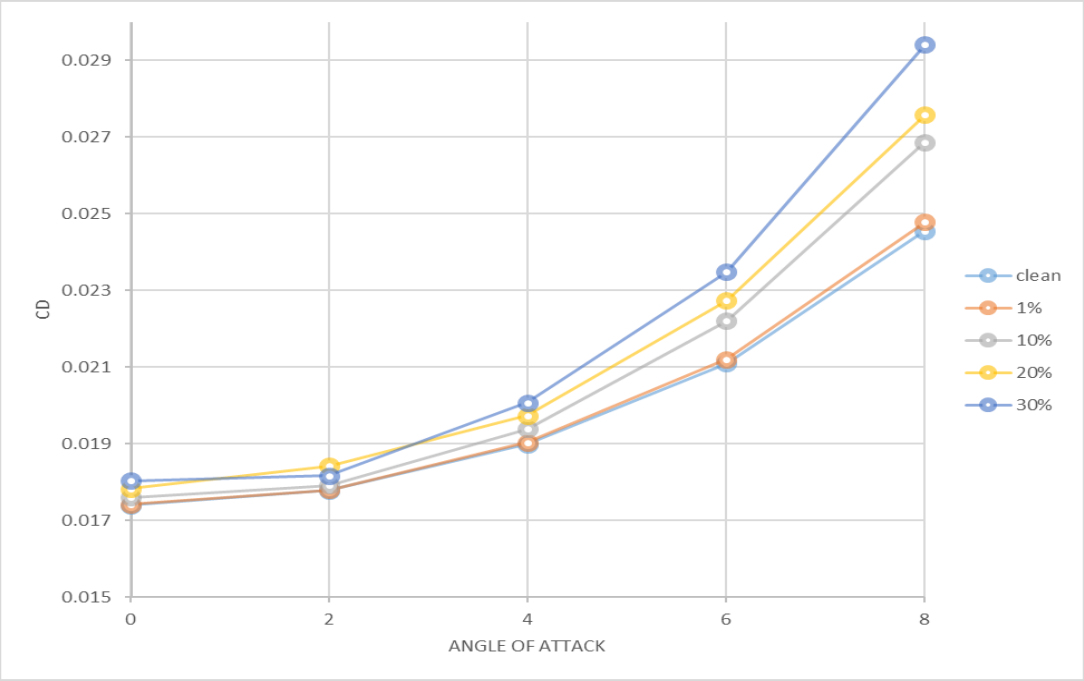

Figure 14: Changes in computed drag coefficient of S809 airfoil under clean air condition for different concentrations of dust particles using realizable k-ε model.

3.5 Pressure, Velocity and Turbulence Intensity Contours and Velocity Vectors

Contours in Figures 15 and 16 display the magnitudes and distribution of pressure and velocity respectively around S809 airfoil at various angles of attack. As mentioned before, at angle of attack = 0, the pressure and velocity distribution on the suction surface (upper surface) and the pressure surface (lower surface) of S809 airfoil are not symmetrical leading to non-zero lift force as expected. As angle of attack becomes larger, the degree of this asymmetry increases resulting in higher lift force. This phenomenon corresponds to the results shown in Figure 8; the discussion is provided in section 3.3 and can be explained by the Bernoulli's principle. It is interesting to note that there is a low-speed area at the trailing edge of S809 airfoil and its size grows with increase in angle of attack. At higher angles of attack, separation takes place on the

upper surface of the airfoil which eventually results in stall and the lift drops [28]. Characteristics of flow separation at low Reynolds numbers have been widely studied and investigated for many decades [29]. Figure 17 shows the change in turbulence intensity for angles of attack between 0 and 12°. Figures 18 and 19 demonstrate how the velocity in the flow field changes as angle of attack increases and eventually the stall appears. As can be seen from Figure 19, when angle of attack is zero, the velocity vectors are almost unidirectional even for near the trailing edge. However, from Figures 20 and 21, it can be seen that angle of attack increases towards the critical angle of attack at which stall occurs, vortices appear on the upper surface near the trailing edge, which increase the turbulence intensity. Figure 20 shows the vortex near the trailing edge of S809 airfoil when angle of attack is 15°, which is larger than the critical angle of attack at which stall occurs. The zoomed-in-view shows the velocity gradient in the boundary layer which also provides a strong evidence that the mesh was adequately refined near the surface of the S809 wind turbine airfoil and gives accurate results.

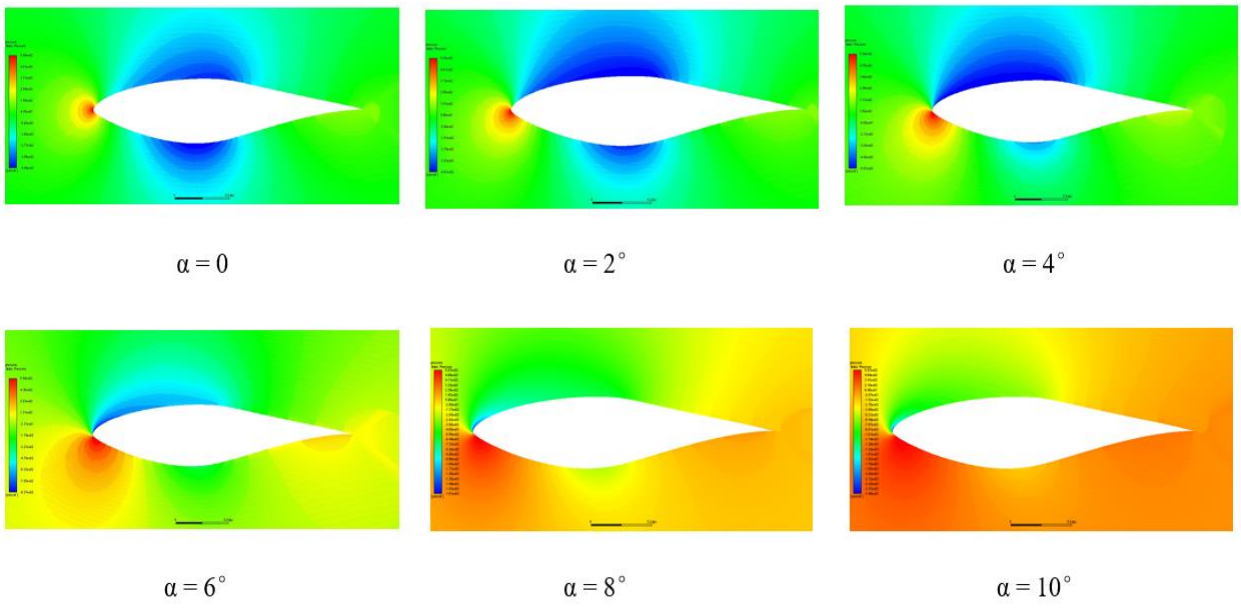

Figure 15: Pressure contours around S809 airfoil at different angles of attack.

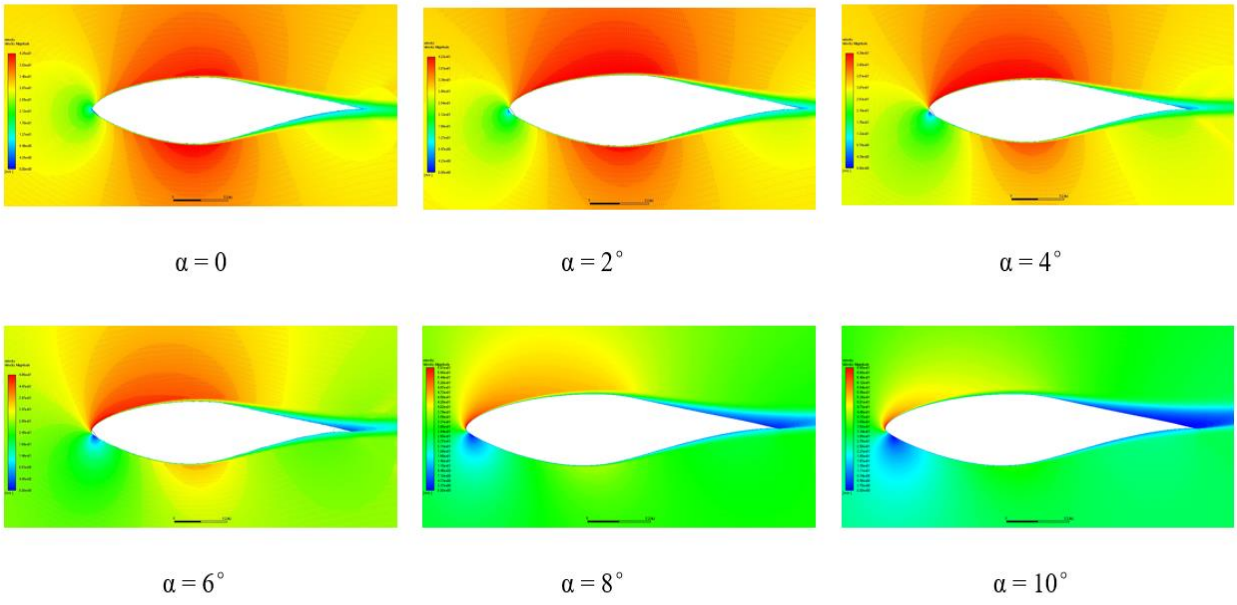

Figure 16: Velocity contours around S809 airfoil at different angles of attack.

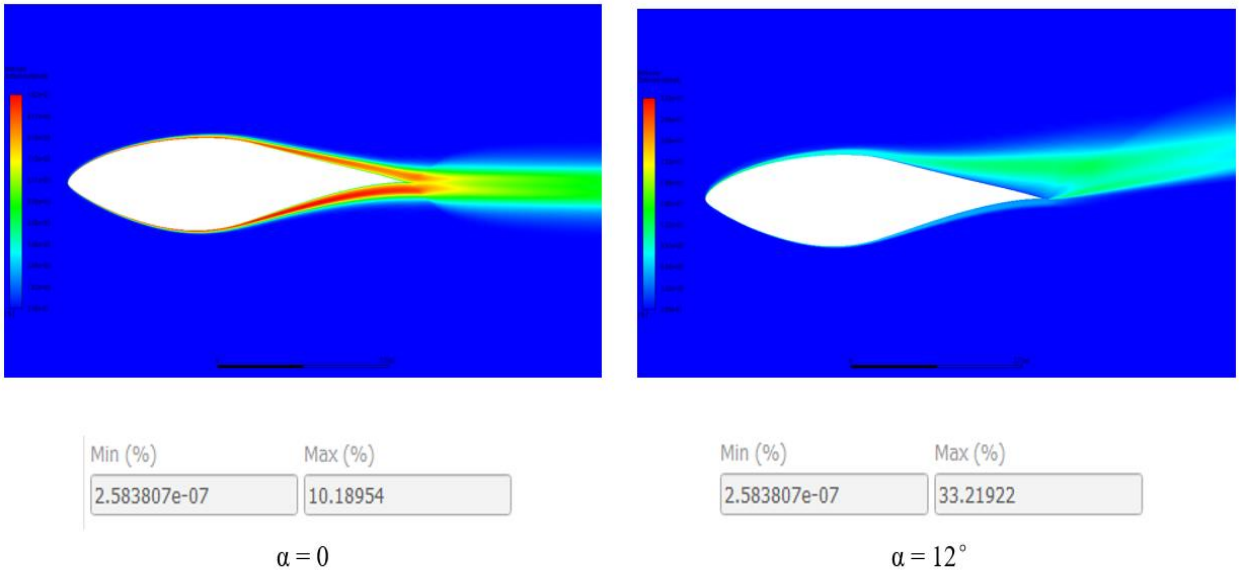

Figure 17: Percentage of turbulence intensity and its contours around S809 airfoil at two angles of attack

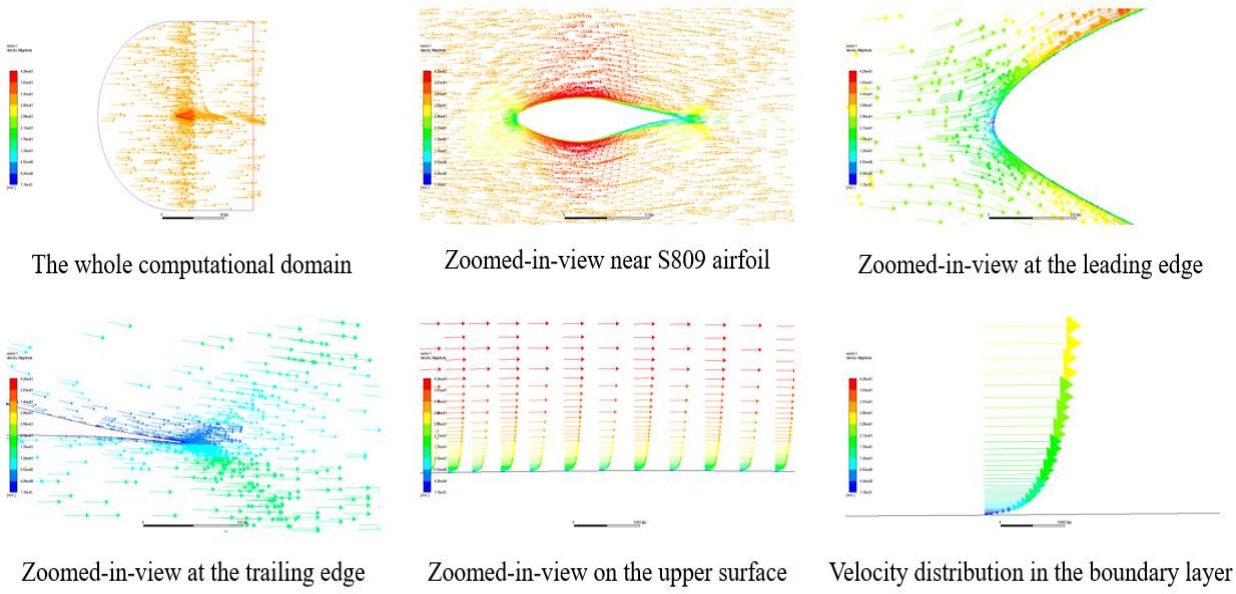

Figure 18: Velocity vectors around S809 airfoil at α=0°.

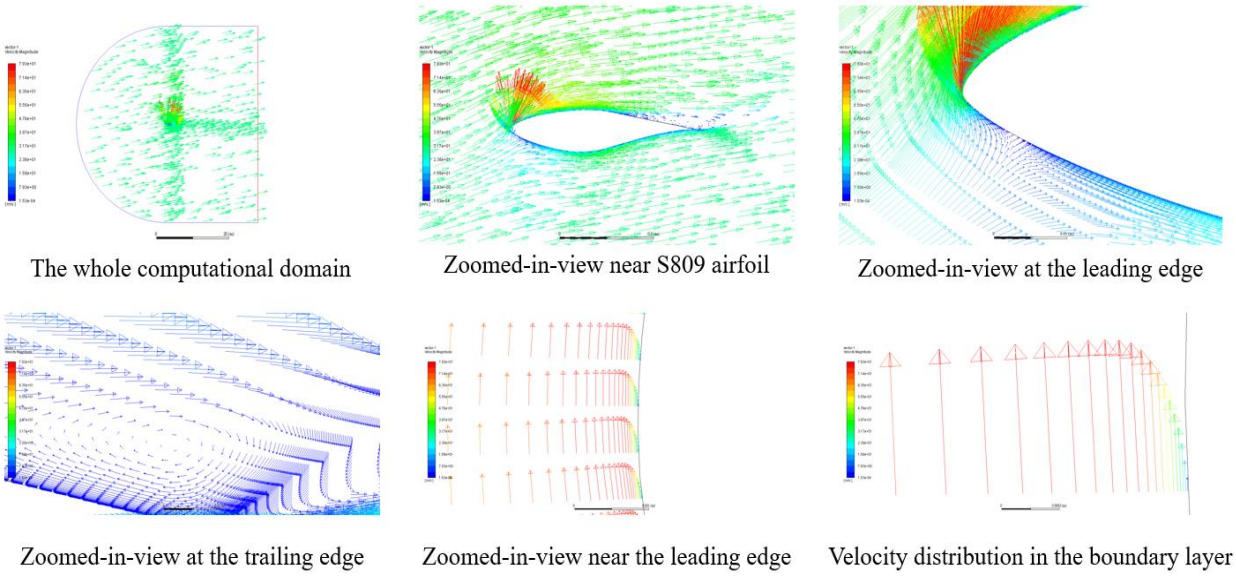

Figure 19: Velocity vectors around S809 airfoil at α=12°.

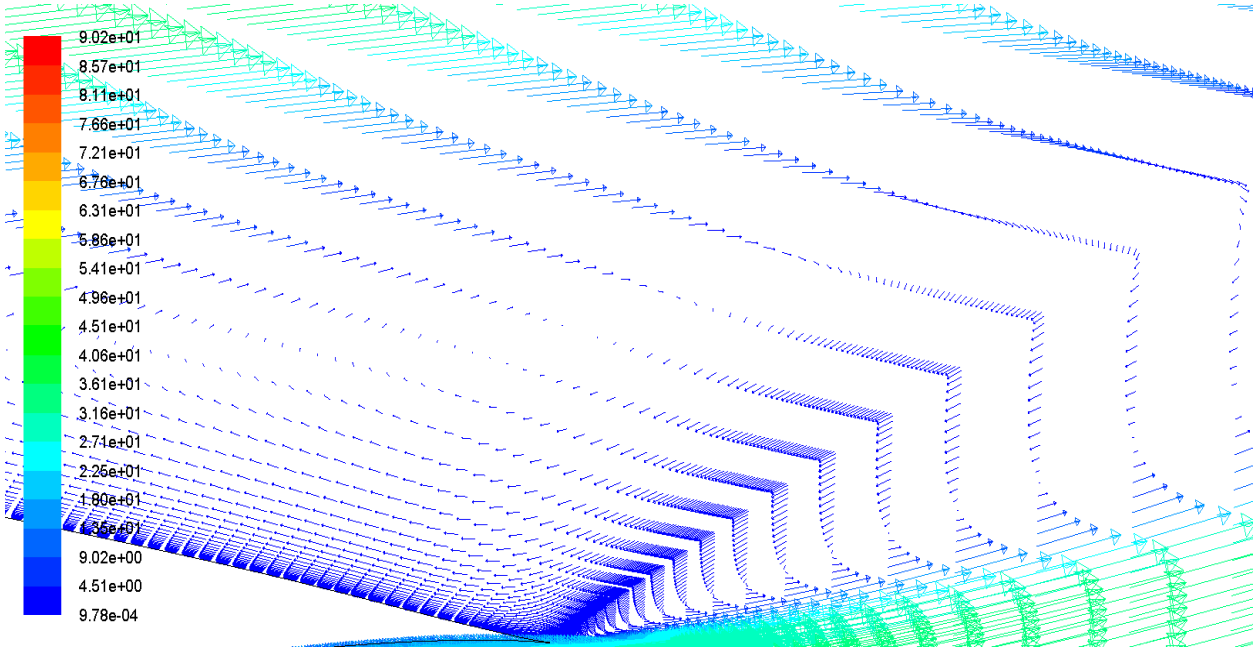

Figure 20: Zoomed-in-view of velocity vectors near the trailing edge of S809 airfoil at α=15°.

Chapter 4: S814 Airfoil

4.1 Basic Information of S814 Airfoil

S814 airfoil is a 24-percent-thick airfoil whose geometry is shown in Figure 20. S814 airfoil was designed to replace S811 airfoil to achieve a transition-free flow with higher maximum lift coefficient.

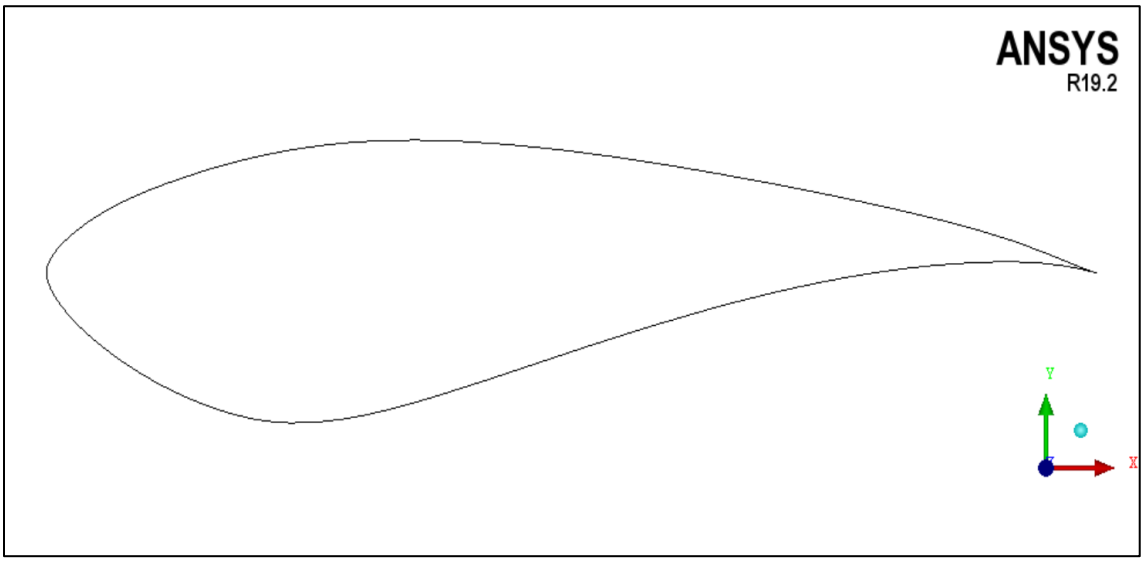

Figure 21: Geometry of S814 airfoil.

4.2 Simulations and Results under Clean Air Condition

Figures 21 and Figure 22 show the computed results for S814 airfoil using SA model, realizable k-ε model and WA 2017m model and their comparison with the experimental data. All three models show good agreement of lift coefficient with the experimental data at lower angles of attack but the deviation between the computed results and experimental data increases when angle of attack increases. This is expected in case of most airfoils. Furthermore, the computed drag coefficient using the three models differs considerably from the experimental data which is also an expected result from CFD. Drag coefficient is higher than experimental data for the entire

range of angles of attack. The reason for large error between computation and experiment could also be due to the inadequacy mesh but it is rather unlikely since mesh was shown to be of very high quality. Linearly dependence of c_l-α at small angle of attack and non-zero lift for angle of attack=0° also exist in case of S814 airfoil as was the case with S809 airfoil.

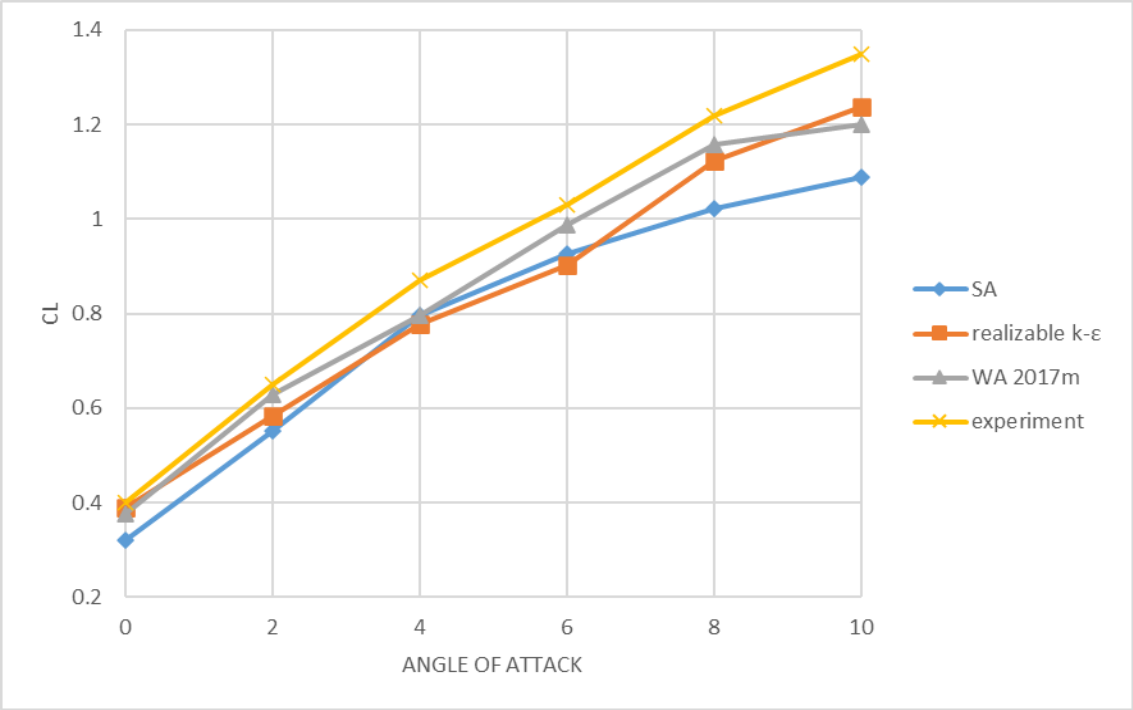

Figure 22: Variation in computed lift coefficients of S814 airfoil under clean air condition using SA model, realizable k-ε model and WA 2017m model and their comparison with experimental data.

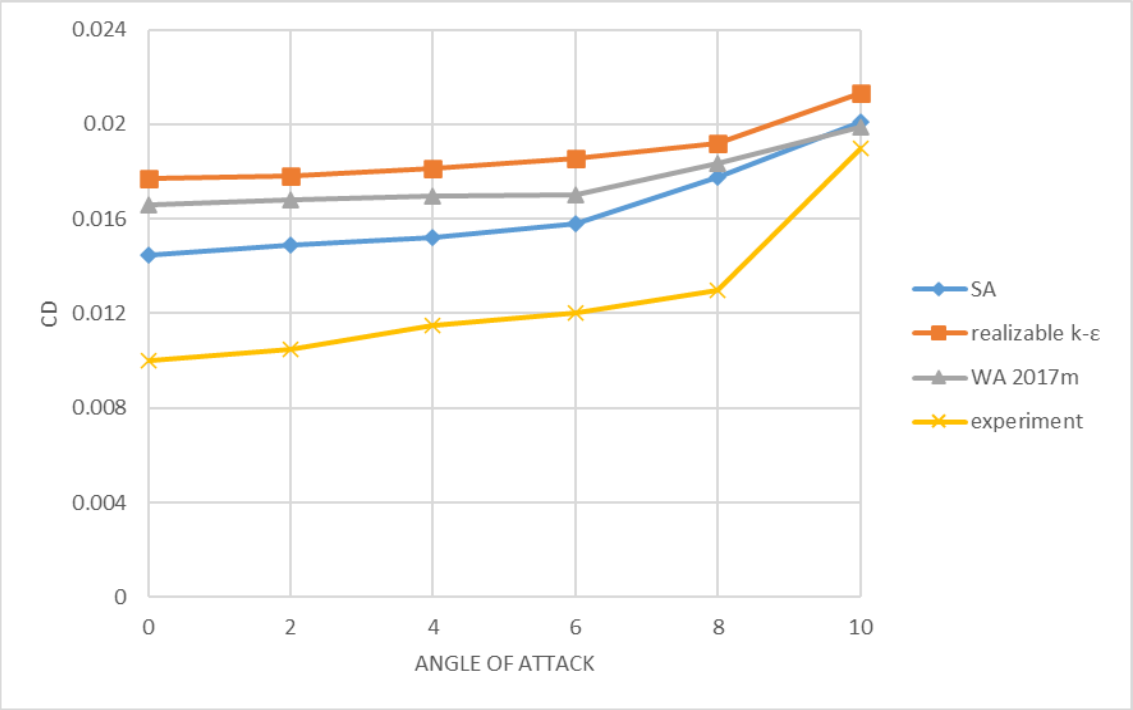

Figure 23: Variation in computed drag coefficients of S814 airfoil under clean air condition using SA model, realizable k-ε model and WA 2017m model and their comparison with experimental data.

4.3 Simulations and Results under Dusty Air Condition

Same as S809 airfoil, simulations are performed for S814 airfoil under dusty air condition by employing the discrete phase model with realizable k-ε model and WA 2017m model; the results are compared with the computations for clean air condition. Figures 24 and 25 show the difference in results using different turbulence models. In all cases the concentration of particles is set at 10% by volume. From these figures, it can be concluded that the trend in aerodynamic characteristics of S814 airfoil is similar to that for S809 airfoil, that is the decrease in lift coefficient and increase in drag coefficient due to the presence of dust particles.

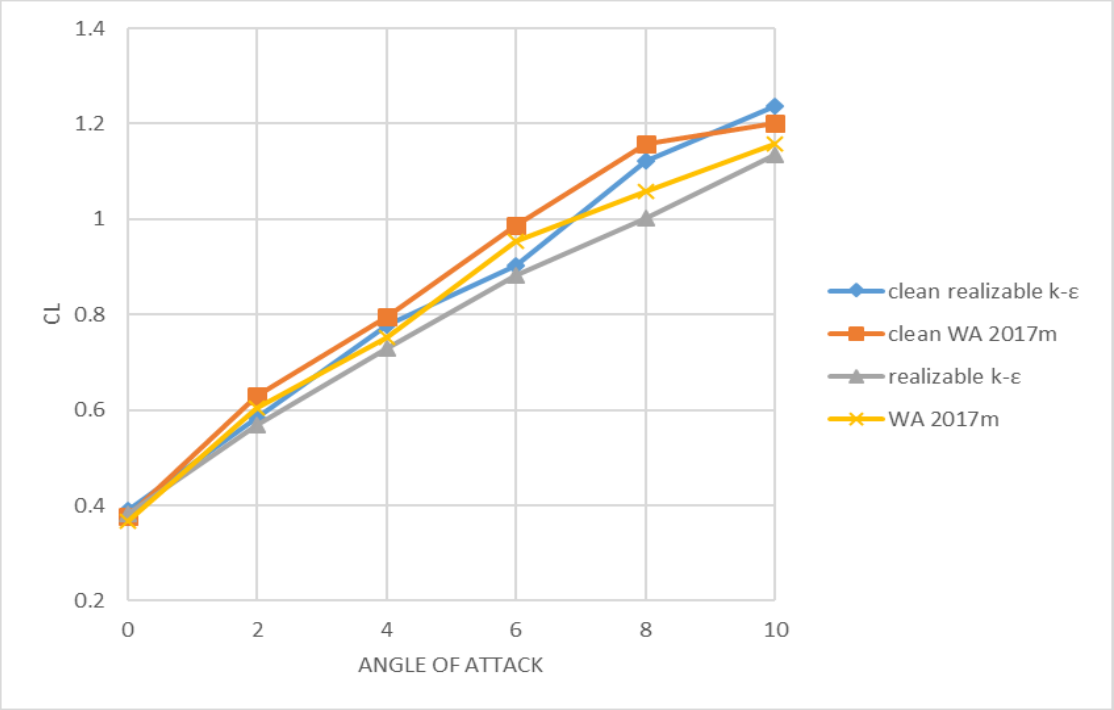

Figure 24: Changes in lift coefficient of S814 airfoil under clean and dusty air conditions using realizable k-ε model and WA 2017m model when concentration of dust particle is 10% by volume.

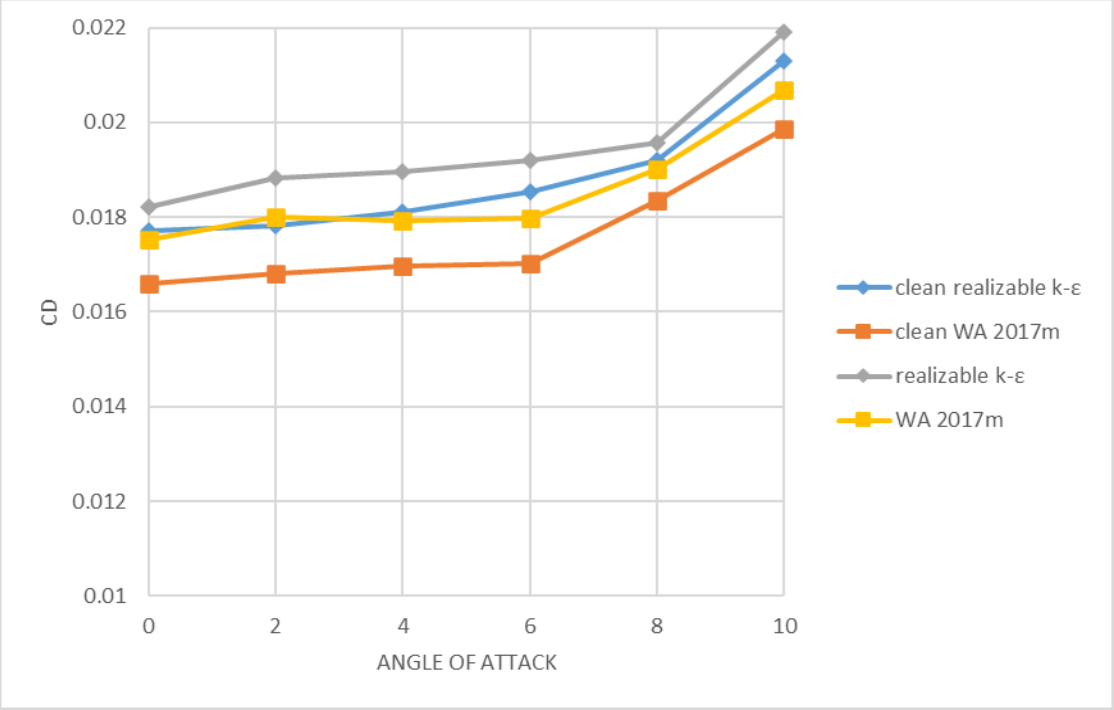

Figure 25: Change in drag coefficient of S814 airfoil under clean and dusty air conditions using realizable k-ε model and WA 2017m model when concentration of dust particle is 10% by volume.

4.4 Pressure, Velocity and Turbulence Intensity Contours

Contours in Figures 26 and 27 show the magnitudes and distribution of the pressure and velocity respectively around S814 airfoil at various angles of attack. Figure 28 shows the change in turbulence intensity for angles of attack of 0 and 10°. As was the case for S809 airfoil, the maximum turbulence intensity is higher for larger angle of attack.

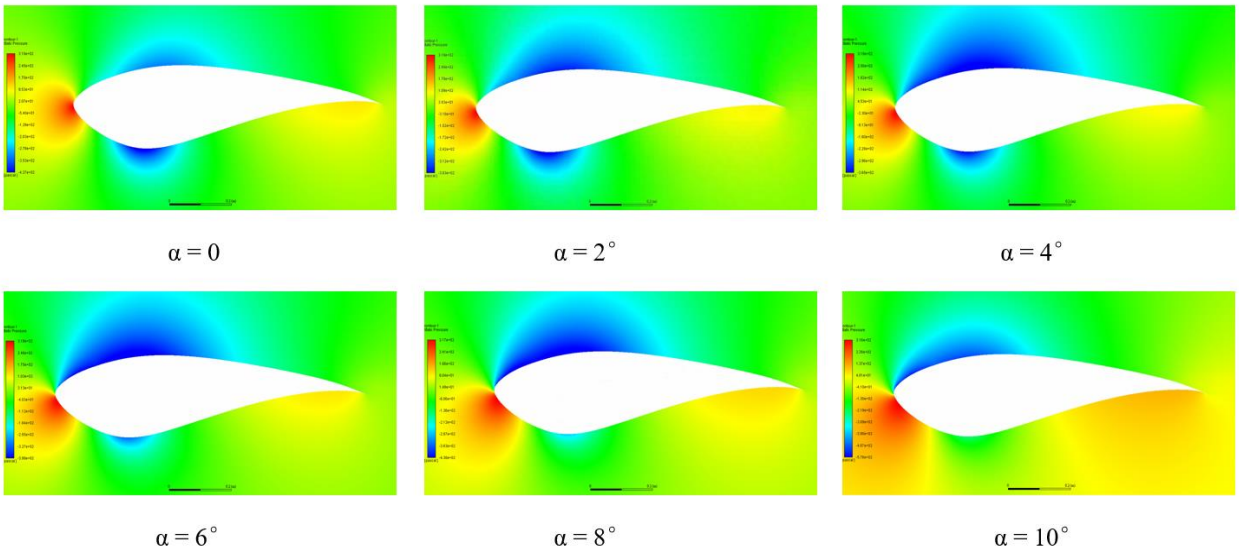

Figure 26: Pressure contours around S814 airfoil at different angles of attack.

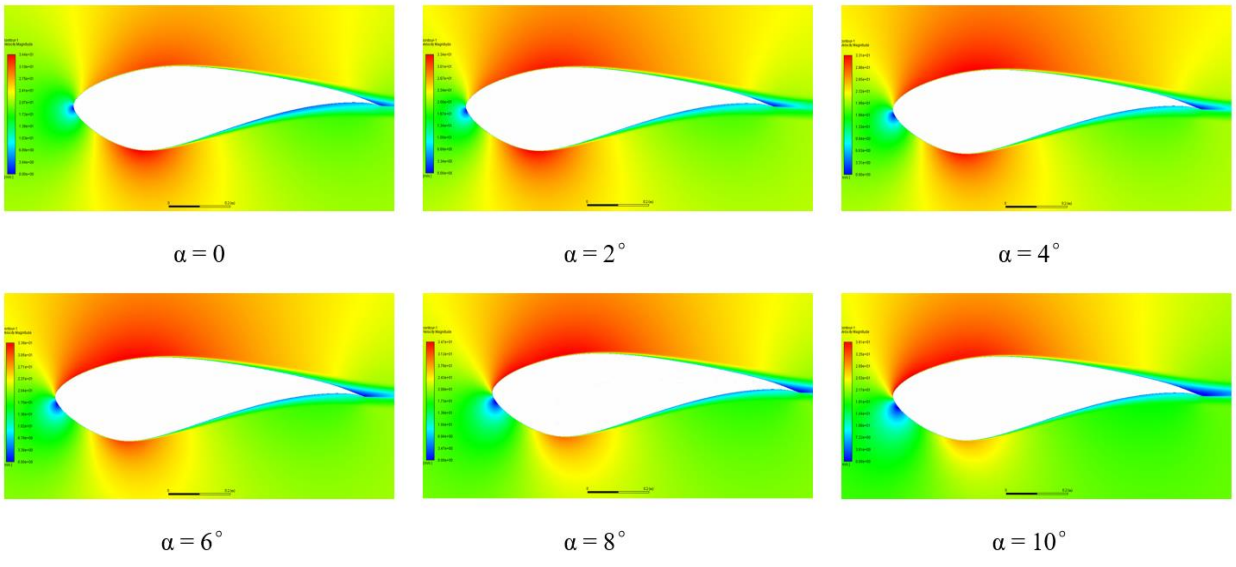

Figure 27: Velocity contours around S814 airfoil at different angles of attack.

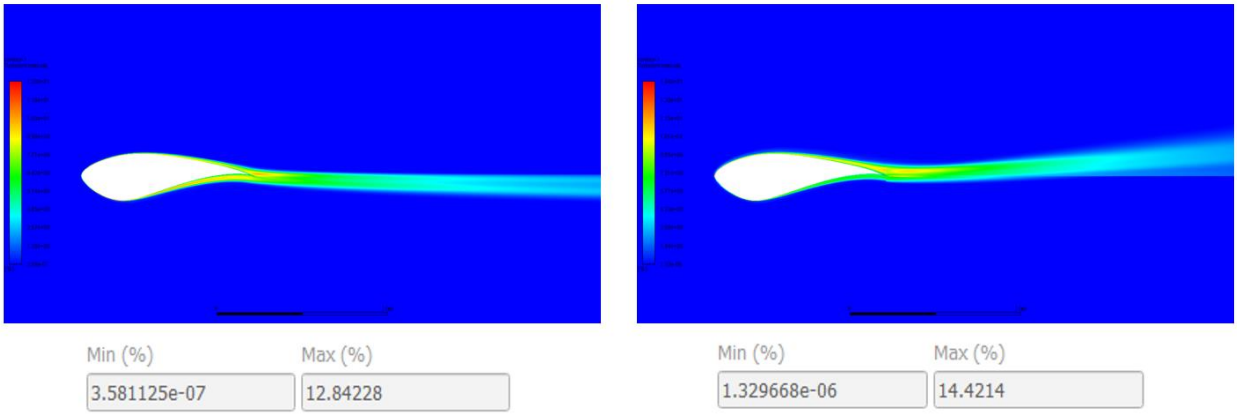

$\alpha = 0$ $\alpha = 10^{\circ}$

Figure 28: Percentage of turbulence intensity and its contours around S814 airfoil at two angles of attack

Chapter 5: S1210 Airfoil

5.1 Basic Information of S1210 Airfoil

S1210 airfoil is a 12-percent-thick low Reynolds number airfoil, whose geometry is shown in Figure 28. This airfoil was designed by Selig at UIUC as one of a series of airfoils designed in the late 1990s for remote-control model aircraft applications, providing high-lift at low Reynolds Numbers [22-25]. S1210 airfoil is a highly-cambered airfoil, as shown in Figure 29. Derivatives of S1210 airfoil, such as S1223 airfoil, have also shown improvements in operational performance of wind turbines for a range of tip speeds [26].

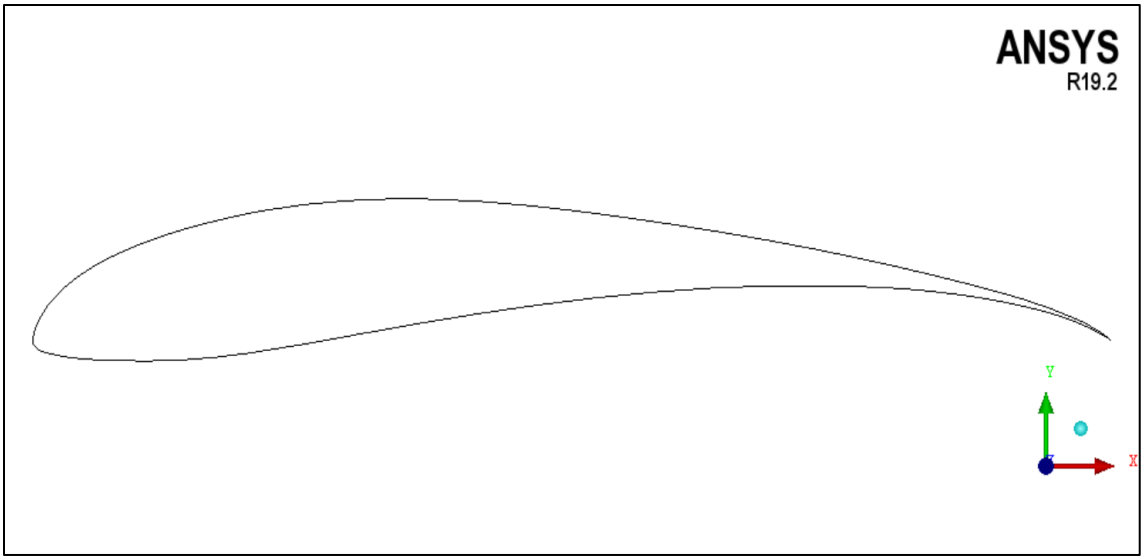

Figure 29: Geometry of S1210 airfoil.

5.2 Simulations and Results under Clean Air Condition

Figures 30 and Figure 31 show the computed results for S1210 airfoil using SA model, realizable k-ε model and WA 2017m model and their comparison with the experimental data. The three turbulence models show good agreement of lift coefficient with the experimental data but larger error for drag coefficient as expected in CFD simulations, as was also the case for S814 airfoil under clean air condition.

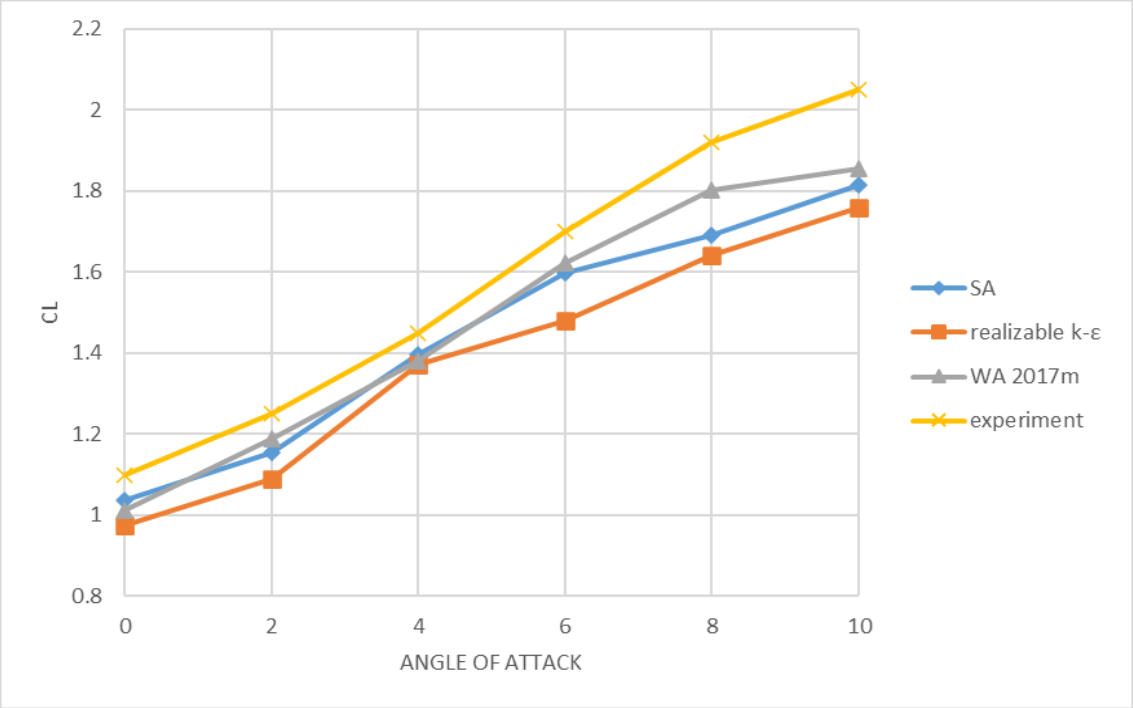

Figure 30: Variation in computed lift coefficients of S1210 airfoil under clean air condition using SA model, realizable k-ε model and WA 2017m model and their comparison with experimental data.

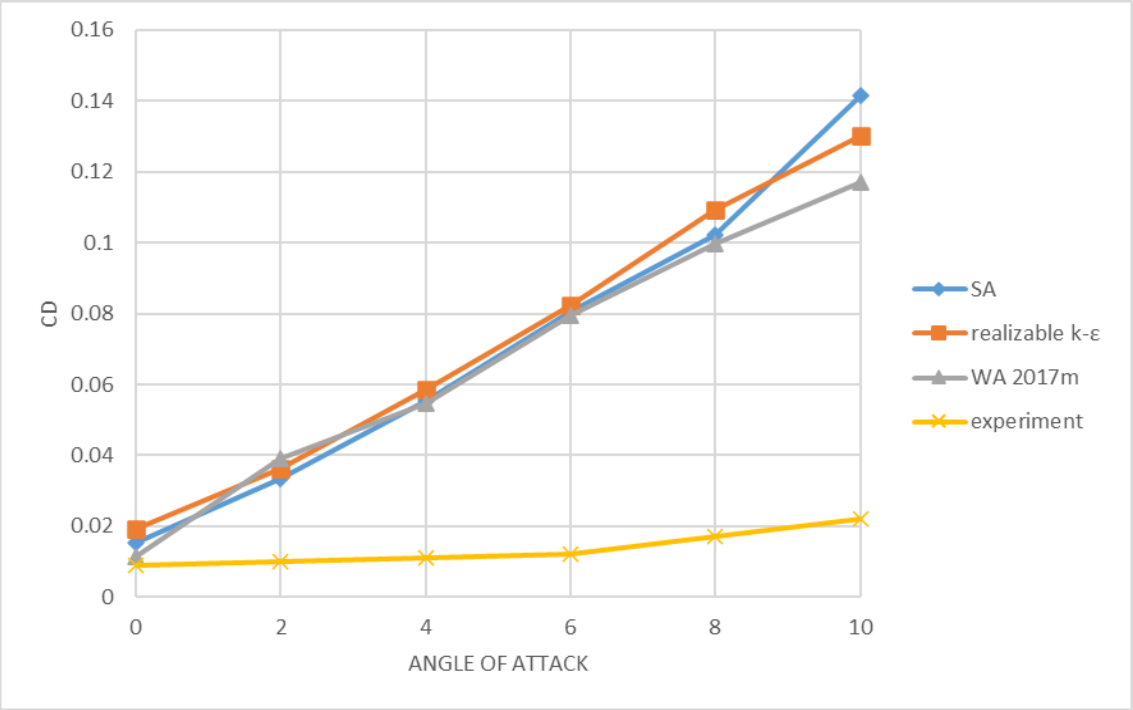

Figure 31: Variation in computed drag coefficients of S1210 airfoil under clean air condition using SA model, realizable k-ε model and WA 2017m model and comparison with experimental data.

5.3 Simulations and Results under Dusty Air Condition

Simulations for flow past S1210 airfoil under dusty air condition are performed using the discrete phase model with realizable k-ε model and WA 2017m turbulence model and are compared with the computed results under clean air condition. Figures 32 and 33 show the difference in results using different turbulence models. In all cases, the concentration of dust particles is 10% by volume. The variation trends in aerodynamic characteristics of S1210 airfoil are the same to those of S809 and S814 airfoils.

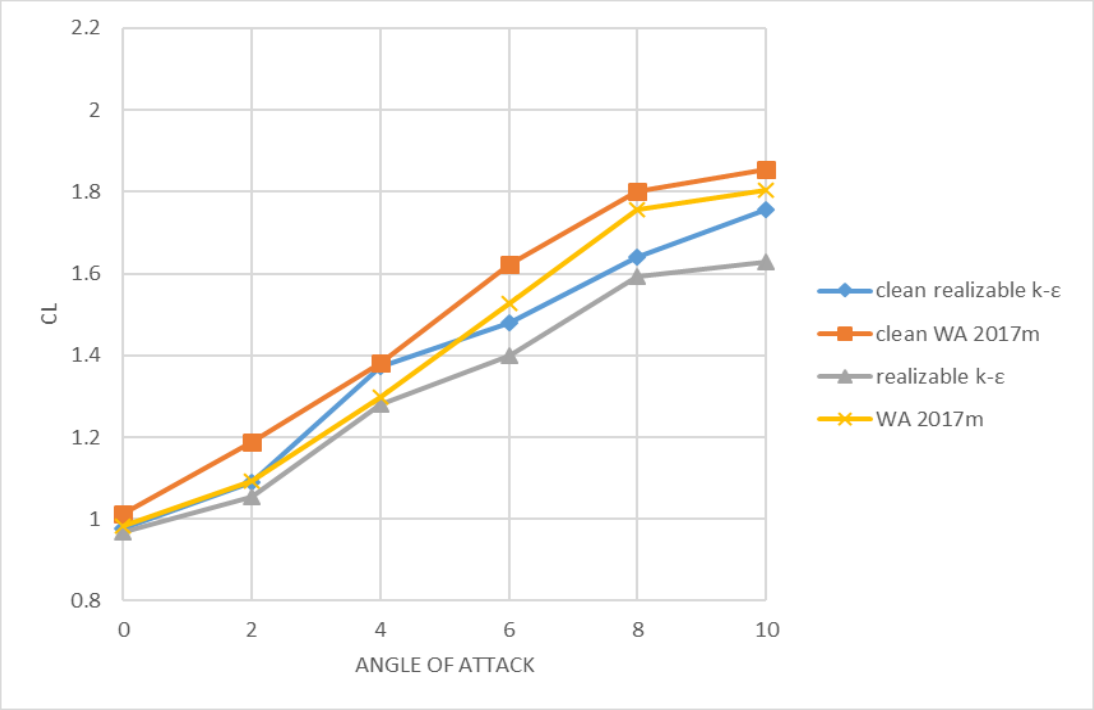

Figure 32: Changes in lift coefficient of S1210 airfoil under clean and dusty air conditions using realizable k-ε model and WA 2017m model when concentration of dust particles is 10% by volume.

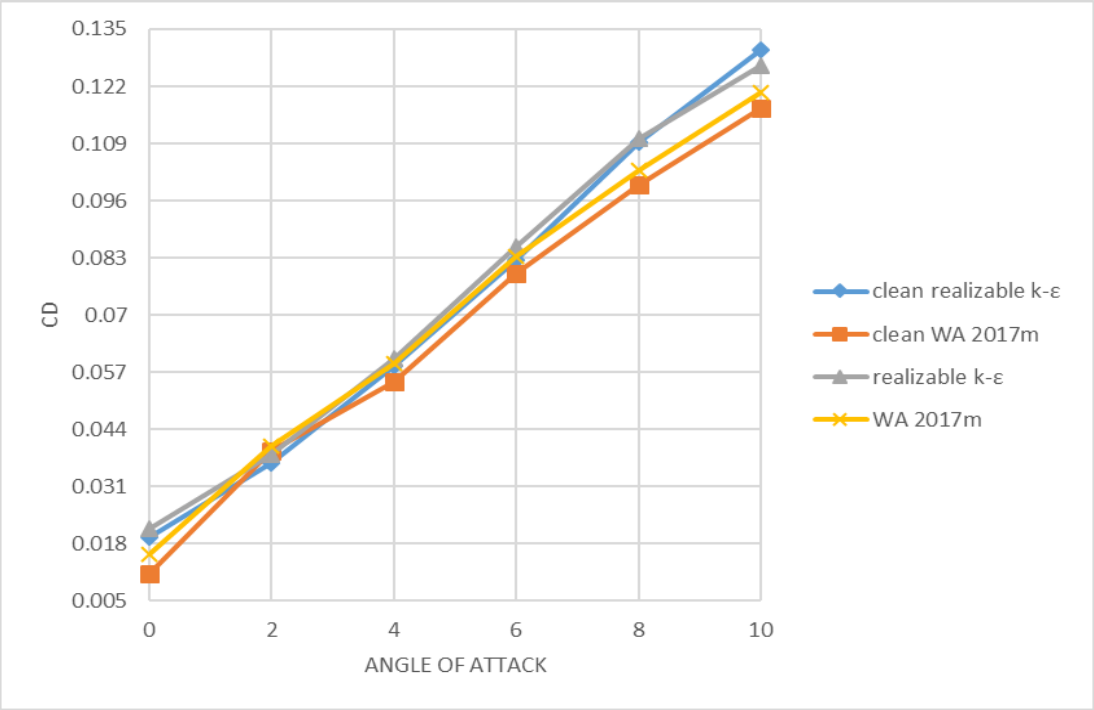

Figure 33: Change in drag coefficient of S1210 airfoil under clean and dusty air conditions using realizable k-ε model and WA 2017m model when concentration of dust particles is 10% by volume.

5.4 Pressure, Velocity and Turbulence Intensity Contours

Contours of Figures 34 and 35 show the magnitudes and distribution of the pressure and velocity respectively around S1210 airfoil at various angles of attack. Figure 36 shows the difference in turbulence intensity at angles of attack of 0 and 10°. It is interesting to note that unlike the S809 and S814 airfoils, the maximum turbulence intensity declines for S1210 airfoil with larger angle of attack.

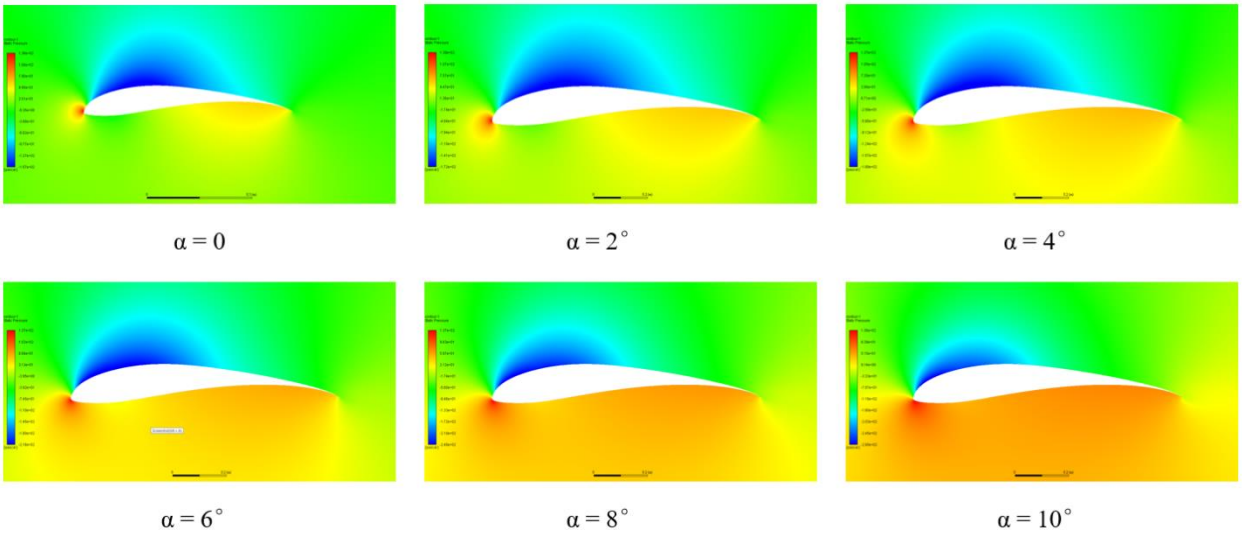

Figure 34: Pressure contours around S1210 airfoil at different angles of attack.

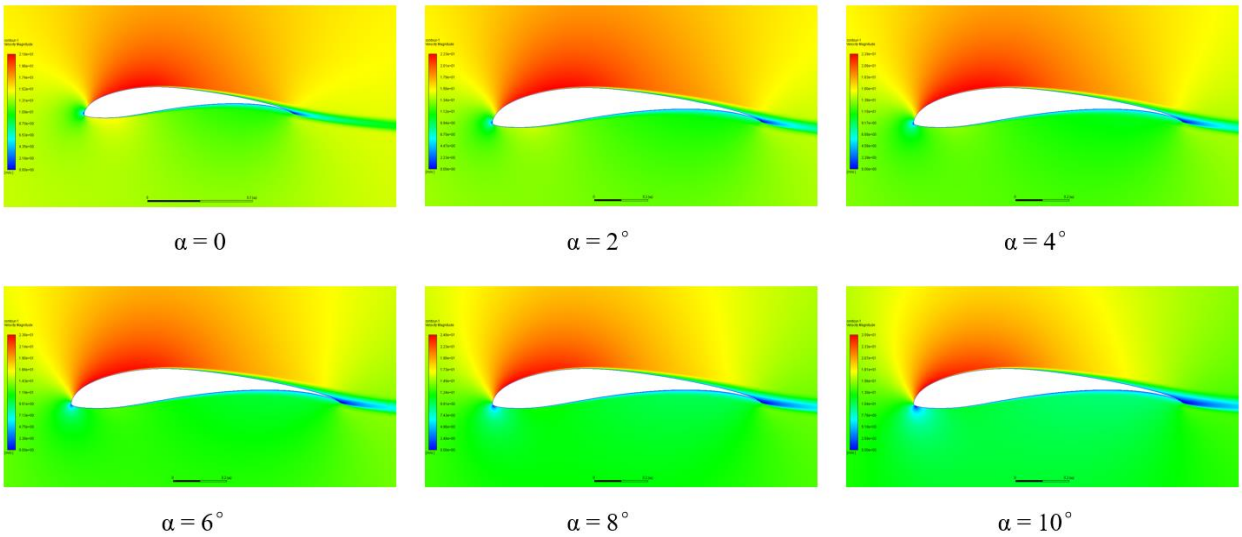

Figure 35: Velocity contours around S1210 airfoil at different angles of attack.

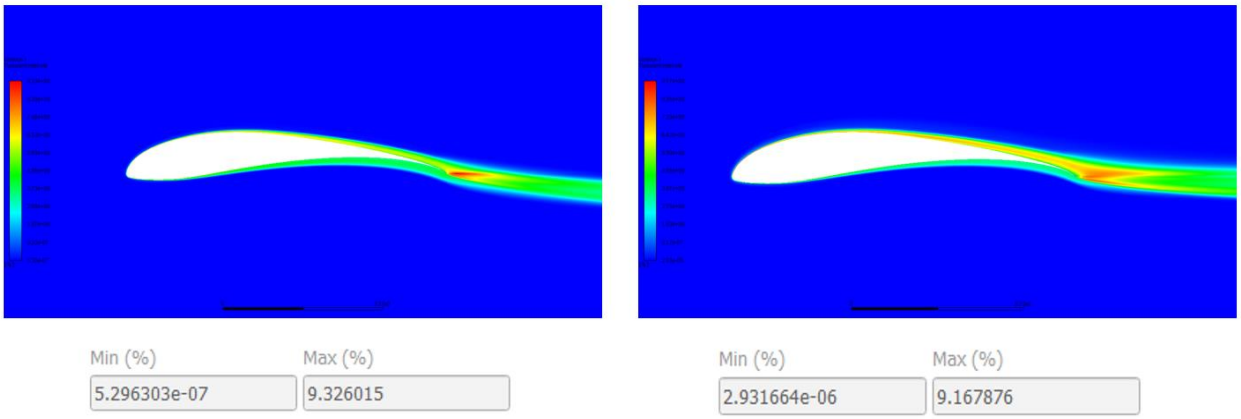

$\alpha = 0$ $\alpha = 10^{\circ}$

Figure 36: Percentage of turbulence intensity and its contours of S1210 airfoil at two angles of attack.

Chapter 6: Conclusions and Future Work

In Chapters 3, 4 and 5, the computational results for S809, S814 and S1210 airfoils were presented. In this chapter, the results for these three airfoils are compared. Figures 37 and 38 show the difference in lift coefficient and drag coefficient among the three airfoils. From these figures, it can be noted that the lift coefficient at same angle of attack for S1210 airfoil is significantly larger than that for S809 and S814 airfoils, which implies that S1210 airfoil has the best aerodynamic performance among these three airfoils.

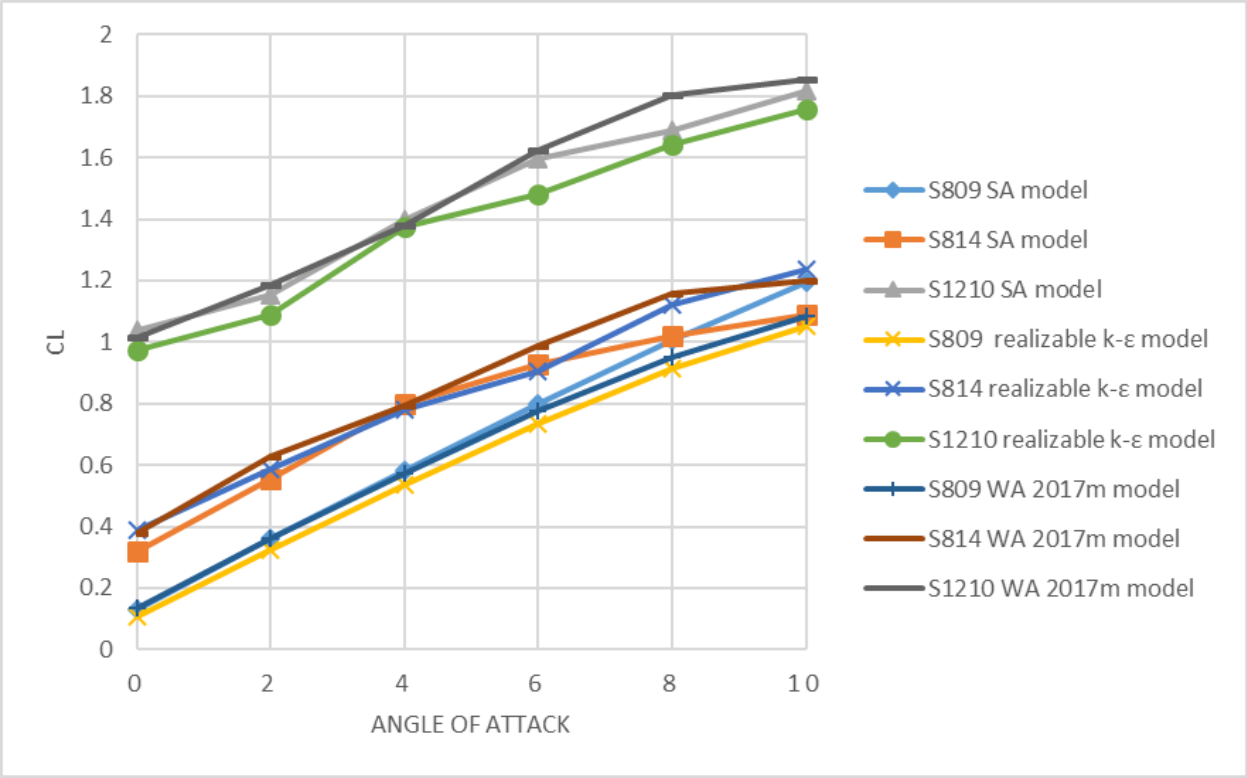

Figure 37: Changes in lift coefficients of three airfoils (S809, S814, S1210) using different turbulence models under clean air condition

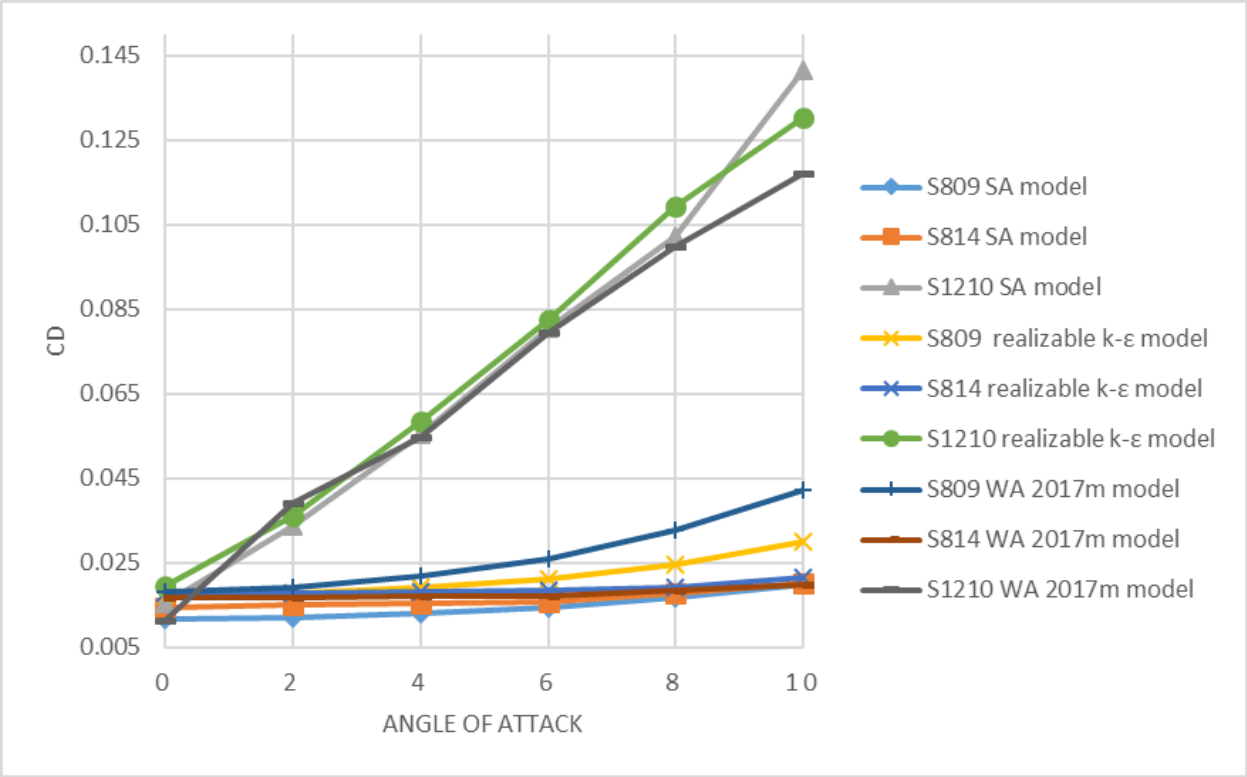

Figure 38: Changes in drag coefficients of three airfoils (S809, S814, S1210) using different turbulence models under clean air condition

To summarize, several conclusions can be drawn based on this research:

1. Aerodynamic performance of wind turbine airfoils is influenced by the usual flow and geometric parameters such as angle of attack, Reynolds number, thickness and camber as well as the conditions of air (clean or dusty).

2. Injection of dust particles can generate negative effects on the aerodynamic performance of the wind turbine airfoils; the drag coefficient increases and the lift coefficient decreases resulting in a lower lift to drag ratio and energy efficiency.

3. Based on the comparison between the results for 1% , 10%, 20% and 30% concentration of dust particles by volume in dusty air, it is found that larger concentration of dust particles has

more detrimental effect on aerodynamic performance as expected and therefore on the power output of the wind turbines.

4. The wind turbines will not only have erosion effect and degradation of blades in dusty environment but also have relatively lower power generation in countries where sand dust is very common in the environment e.g. countries in the Middle East.

Other than dusty air condition, there are also several other aspects which can influence the aerodynamic performance of airfoils:

1. The surface of airfoils can be eroded by the impact of solid particles and the roughness resulting from the erosion will have negative effect.

2. The research from NASA found out that ice accretion on the surface of airfoils, especially near the leading edge, can also reduce the efficiency of airfoils.

3. In spite of the external factors, the material strength and toughness of airfoils are also critical for good performance.

More study and research is needed to determine how these factors influence the aerodynamic performance of airfoils so that effective improvements in the blade design can be accomplished to better utilize the wind energy.

References

[1]. K. Pope, I. Dincer, and G.F. Naterer, "Energy and Exergy Efficiency Comparison of Horizontal and Vertical Axis Wind Turbines," Renewable Energy, Vol. 35, 2010, pp.2102-2113.

[2]. M.R. Islam, L.B. Bashar, D.K. Saha, and N.S. Rafi., "Comparison and Selection of Airfoils for Small Wind Turbine between NACA and NREL's S-series Airfoil Families," International Journal of Research in Electrical, Electronics and Communication Engineering, Vol 4, 2019, pp.1-12.

[3]. J.L. Tangier and D. M. Somers, "NREL Airfoil Families for HAWTs," National Renewable Energy Laboratory,TP-442-7109, January 1995.

[4]. D.M. Somers, "Design and Experimental Results for the S809 Airfoil," National Renewable Energy Laboratory, SR-440-6918, January 1997.

[5]. D.M. Somers, "Design and Experimental Results for the S814 Airfoil," National Renewable Energy Laboratory, SR-440-6919, January 1997.

[6]. M.S. Selig, J. J. Guglielmo, A.P. Broeren and P. Giguere., "Summary of Low-Speed Airfoil Data," University of Illinois at Urbana-Champaign, Vol. 1, 1995, 95-69524, ISBN 0-9646747-1-8.

[7]. D.B. Stringer, P. Hartman, D.W. Bunner, "A New 360° Airfoil Model for Predicting Airfoil Thrust Potential in Vertical-Axis Wind Turbine Designs," Journal of Renewable and Sustainable Energy, Vol.10, 2018, pp.013304.

[8]. D.C. Douvi, D.P. Margaris, and A.E. Davaris, “Aerodynamic Performance of a NREL S809 Airfoil in an Air-Sand Particle Two-Phase Flow”, MDPI, Computation, Vol. 5, 2017, p.13.

[9]. P.R. Spalart, S.R. Allmaras, “A One -Equation Turbulence Model for Aerodynamic Flows”, AIAA 30th Aerospace Sciences Meeting and Exhibit, 1992, https://doi.org/10.2514/6.1992-439.

[10]. X. Han, T. Wray, R.K. Agarwal, “Application of a New DES Model Based on Wray-Agarwal, Turbulence Model for Simulation of Wall-Bounded Flows with Separation,” AIAA 2017-3966, AIAA 47th AIAA Fluid Dynamics Conference, 2017.

[11]. Yi O., K.-L. Tang, Y. Xiang, H.-K. Zou, G.-Wen Chu, R.K. Agarwal, and J.-F. Chen, “Evaluation of Various Turbulence Models for Numerical Simulation of a Multiphase System in a Rotating Packed Bed,” Computers and Fluids, Vol.13, 2019, p.104296.

[12]. X. Han, T.J. Wray, C. Fiola, and R.K. Agarwal, “Computation of Flow in S Ducts with Wray–Agarwal One-Equation Turbulence Model,” J. Propulsion and Power, Vol. 31, 2015, pp. 1338–1349. doi:10.2514/1.B35672.

[13]. S.B. Pope, "Turbulent flows." Cambridge University Press (2001): 2020.pp. 3-5, https://doi.org/10.1017/CBO9780511840531.

[14]. H. Gopalan., “Evaluation of Wray-Agarwal Turbulence Model for Simulation of Neutral and Non-Neutral Atmospheric Boundary Layers,” Journal of Wind Engineering and Industrial Aerodynamics, Vol.182, 2018, pp.322-329.

[15]. A. Sokolichin and G. Eigenberger., "Dynamic Numerical Simulation of Gas-Liquid Two-Phase Flows Euler/Euler Versus Euler/Lagrange," Chemical Engineering Science, Vol. 52, 1997, pp.611-626.

[16]. T. Wan and S.-P. Pan, "Aerodynamic Efficiency Study under the Influence of Heavy Rain via Two-Phase Flow Approach", 27th International Congress of the Aeronautical Sciences, Vol. 2, 2010, pp.1343-1353

[17]. ANSYS Fluent Theory Guide, Chapter 16: Discrete Phase Model, November 2013.

[18]. R.R. Ramsay, M.J. Hoffmann, and G.M. Gregorek "Effects of Grit Roughness and Pitch Oscillations on the S809 Airfoil," National Renewable Energy Laboratory, TP-442-7817, 1995.

[19]. M.J. Barnsley and J.F. Wellicome, "Wind Tunnel Investigation of Stall Aerodynamics for a 1.0 m Horizontal Axis Rotor", Journal of Wind Engineering and Industrial Aerodynamics, Vol. 39, 1992, pp.11-21.

[20]. J.D. Anderson, Jr. "Fundamentals of Aerodynamics" Sixth Edition, McGraw-Hill Education, 2017.

[21]. S. Jain, N. Sitaram, and S. Krishnaswamy, "Effect of Reynolds Number on Aerodynamics of Airfoil with Gurney Flap", Hindawi Publishing Corporation, International Journal of Rotating Machinery, Vol. 2015, 2015, DOI:10.1155/2015/628632.

[22]. C. A. Lyon, A. P. Broeren, P. Giguere, A. Gopalaratham, and M. Selig, "Summary of Low-Speed Airfoil Data", University of Illinois at Urbana-Champaign, Vol. 3. 1997.

[23]. M. S. Selig and J. J. Guglielmo, “High-Lift Low Reynolds Number Airfoil Design,” J. Aircraft, Vol. 34, 1997, pp.72–79.

[24]. M. S. Selig, C. A. Lyon, P. Giguere, and J. J. Ninham, and C.P. Guglielmo, “Summary of Low-Speed Airfoil Data,” Vol. 2, 1996, ISBN 0-9646747-2-6.

[25]. M. Selig, J. J. Guglielmo, A. P. Broeren, and P. Giguere, “Summary of Low-Speed Airfoil Data”, Vol. 1, 1995, 95-69524, ISBN 0-9646747-1-8.

[26]. P. Chougule and S. Nielsen, “Overview and Design of Self-Acting Pitch Control Mechanism for Vertical Axis Wind Turbine Using Multi-Body Simulation Approach,” Journal of Physics: Conference Series, Vol. 524, 2014.

[27]. J. Winslow, H. Otsuka, B. Govindarajan, and I. Chopra “Basic Understanding of Airfoil Characteristics at Low Reynolds Numbers,” Journal of Aircraft, Vol. 55, 2018, pp.104-105.

[28]. L. Juanmian, G. Feng, H. Can “Numerical Study of Separation on the Trailing Edge of a Symmetrical Airfoil at a Low Reynolds Number,” Chinese Journal of Aeronautics, vol. 26, 2013, pp.918-915.

[29]. H.P. Horton, “Laminar Separation Bubbles in Two and Three Dimensional Incompressible Flow,” PhD dissertation, University of London, 1968.

[30]. “S1210 12% - Selig S1210 High Lift Low Reynolds Number Airfoil” Retrieved from http://airfoiltools.com/plotter/index?airfoil=s1210-il.

Curriculum Vita

Siyuan Chen

EDUCATION

M.S. in Mechanical Engineering, Department of Mechanical Engineering and Materials Science, Washington University in St. Louis, Saint Louis, MO, USA, 2018-2020

Exchange student, Department of Energy Power and Mechanical Engineering, Harbin Institute of Technology, Harbin, China, 2015-2016

B.S. in Energy and Power Engineering, Department of Energy Power and Mechanical Engineering, Dalian University of Technology, Dalian, China, 2013-2017

PUBLICATIONS

Siyuan Chen and Ramesh Agarwal, "Numerical Investigation of Wind Turbine Airfoils under Clean and Dusty Air Conditions," 2020 AIAA Aviation and Aeronautics Forum and Exposition, Reno, NV, June 2020.